# Multi-behavioral phenotyping in zebrafish identifies a novel disruptor of non-associative learning with environmental and human relevance


## Abstract

The vertebrate nervous system is vulnerable to chemical toxicity and the widespread release of chemicals into the environment outstrips the capacity to assess their safety. We devised a battery of automated behavior assays in larval zebrafish (*Danio rerio*), a 3R-compliant model amenable to higher-throughput chemical screens. The battery captures stereotypical visual and acoustic behaviors including habituation, a form of non-associative learning. Known pharmacological modulators of habituation in zebrafish evoked distinct behavioral patterns. By screening chemicals positive for *ex vivo* N-methyl-D-aspartate receptor (NMDAR) modulation, we identified chlorophene, a biocide that caused sedation, paradoxical excitation, and reduced habituation in zebrafish. Using *in silico* target predictions and pharmacological interventions, we discovered that chlorophene acts via gamma-aminobutyric acid A receptors ($GABA_A$Rs), a previously unknown target site. Orthogonal validation in cultured mouse cortical neurons and human stem cell-derived BrainSpheres confirmed chlorophene's interaction with $GABA_A$Rs. Together, multi-behavioral phenotyping in zebrafish can accelerate the identification of neurotoxicants and their underlying mode of action.


## Main

The planetary boundary for chemical pollution has been exceeded based on the concept that the production and release of chemicals outstrips the capacity to monitor human and environmental exposure levels and to perform adequate safety assessments[1]. The global inventory of registered chemicals and mixtures used in commerce totals more than 350,000 substances[2]. The widespread release of anthropogenic chemicals into air, land, and water represents an existential threat to environmental and human health as chemical pollution represents a significant environmental risk factor for disease and premature death[3,4]. The nervous system is one of the most vulnerable organ systems to toxic injury due to the interdependence of neurodevelopmental processes and where perturbations can result in profound structural and/or functional consequences[5]. Epidemiological studies indicate that exposure to pesticides (e.g. rotenone, paraquat, chlorpyrifos), metals (e.g. lead, mercury), neuroactive drugs (e.g. benzodiazepines, anticholinergics), or industrial chemicals (e.g. polychlorinated biphenyls, brominated flame retardants, phthalates) contributes to neurobehavioral pathologies such as Parkinson's disease[6,7], Alzheimer's disease[8–10], attention deficit hyperactivity disorder[11,12], and other neurodevelopmental deficits[13]. These associations are supported by experimental findings in mice[14–18], rats[19,20], non-

human primates[21,22], and other, non-mammalian models[23,24]. Despite these associations, most neurotoxicants remain unknown[13]. This is highlighted by the fact that, to date, fewer than 200 chemicals[25] have been tested according to guideline neurotoxicity studies including acute (28 d), sub-chronic (90 d), and chronic (≥1 year) adult neurotoxicity[26] and developmental neurotoxicity (DNT) studies[27,28]. This lack of information exists because DNT *in vivo* studies are typically conducted in rats[27,28], costly (~$1,000,000 per chemical[29]), laborious (~1 year per chemical[29,30]), and raise ethical concerns[29,31].

As untested chemicals should not be presumed safe, a new testing paradigm is needed to assess the ever-expanding universe of potentially neurotoxic chemicals[13,29]. To fill this gap, an integrated testing strategy that combines *in silico* models, *in vitro* techniques, and alternative animal models, collectively referred to as New Approach Methods (NAMs), has been proposed[29,32,33]. *In silico* methods (e.g. grouping and read-across, quantitative structure-activity relationships) can be used to predict ADME (Absorption, Distribution, Metabolism, Excretion) processes (e.g. blood-brain-barrier penetration), to model physiologically-based toxicokinetics, and to predict mechanisms based on relationships between chemical structure/properties and biological activity[34]. *In silico* approaches rely on experimental data. International efforts to enhance neurotoxicity testing involve the establishment of a DNT *in vitro* testing battery that depicts key neurodevelopmental processes including proliferation, migration, differentiation, apoptosis, neurite outgrowth, synaptogenesis, and functional network formation in a suite of rodent- and human-based cell models[35,36]. The underlying assumption of this approach is that the alteration of any of these processes is indicative of DNT[35]. Despite advances in depicting the processes that orchestrate nervous system development and function *in vitro*, more complex functional endpoints at the organismal level, including complex behaviors, remain elusive. In particular, *in vitro* assays fail to capture behavior endpoints assessed in guideline DNT studies including motor activity, motor and sensory function, learning, and memory[27].

The zebrafish is a powerful vertebrate model that can bridge the gap between *in vitro* and mammalian-based *in vivo* studies. Although zebrafish are phylogenetically more distant from humans than rodents, 70% of human genes and 82% of disease-associated human genes have a zebrafish orthologue[37]. Embryo-larval stages of zebrafish up to 5 d post fertilization (dpf) are non-protected[38,39] and therefore considered to be an alternative to mammalian testing[40]. The high reproduction rate, rapid *ex utero* development, and small size of embryo-larval stages make zebrafish amenable to medium-to-high-throughput screens. Early life-stage zebrafish provide a diverse repertoire of behaviors such as spontaneous tail contractions[41], touch-evoked responses[42,43], visual and acoustic startle responses[44], phototaxis[45], learning and memory[46,47].

While multi-behavioral phenotyping in zebrafish has been widely applied in drug discovery[48,49], molecular target identification[50,51], and to study neurological disorders[52–54], the behavior-rich repertoire of zebrafish has yet to be fully deployed to identify and characterize chemicals that cause neurotoxicity.

The aim of this study is to identify and mechanistically evaluate chemical compounds that cause deficits in learning and memory. First, we developed a multi-behavioral phenotyping battery in early-life stage zebrafish to quantify various visual and acoustic behaviors including non-associative learning. Second, we validated the assay battery using known pharmacological modulators of habituation learning. Third, we performed a targeted chemical screen to identify chemical compounds that affect learning and memory in zebrafish. We then combined pharmacological interventions and electrophysiology in mouse- and human-based models to identify mechanisms underlying phenotypic changes and to demonstrate cross-species relevance. Overall, the zebrafish-based multi-behavioral phenotyping approach represents an efficient tool for the identification and mechanistic elucidation of neurotoxic environmental chemicals with relevance across taxa, including humans.

## Results

### A multi-behavioral phenotyping approach to quantify visual and acoustic behaviors in larval zebrafish

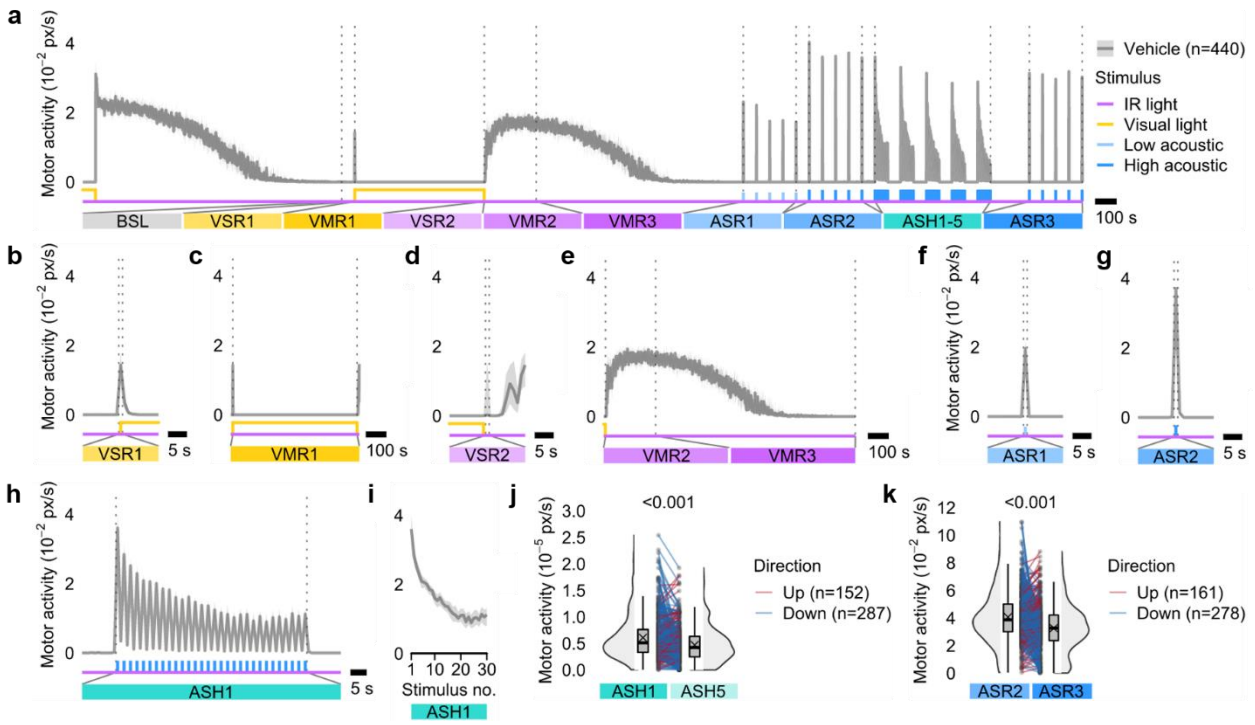


**Figure 1 | A battery of visual and acoustic assays provokes stereotyped behaviors in larval zebrafish.** (**a**) Motor activity (y-axis) of zebrafish larvae over time and across various stimulus modalities (x-axis). Data are median ± 95% CI for *n* = 440 larvae obtained from 28 x 96-well plates, each containing 12-16 control individuals. (**b**) A rapid dark-to-light transition caused a visual startle response (VSR1). (**c**) Subsequent exposure to visual light caused freezing behavior in zebrafish larvae (VMR1). (**d**) Light-to-dark transition caused an additional visual startle response (VSR2). (**e**) Motor activity upon light-to-dark transition reached a maximum after approximately 4 min (VMR2) followed by an asymptotic decrease to baseline (VMR3). (**f**) A series of five low- and (**g**) high-intensity acoustic stimuli (1 s) provokes acoustic startle responses with lower or higher amplitude, respectively. (**h**) A sequence of 30 high-intensity acoustic stimuli (inter stimulus interval, ISI = 1 s) induced an exponential response decrement, indicating habituation. (**i**) Representative plot of data used for **h**, excluding ISIs. (**j**) Decrease in responsiveness during first (ASH1), relative to fifth habituation bout (ASH5), indicates potentiation of habituation. (**k**) Responsiveness to non-habituating high-intensity acoustic stimuli is significantly reduced comparing pre- (ASR2) and post-habituation (ASR3) assays, indicating memory retention. Numbers above the split rainclouds in **j** and **k** represent p-values (one-sided Wilcoxon signed rank exact test). ASH, acoustic startle habituation; ASR, acoustic startle response; BSL, baseline motor activity; VMR, visual motor response; VSR, visual startle response. N=439-440.

To identify chemicals that modulate learning and memory in larval zebrafish, we devised a battery of 11 automated, sequential behavioral assays called the Visual and Acoustic Motor Response (VAMR) assay battery. The battery included assays which quantified baseline (BSL) activity, visual

startle responses (VSR1,2), visual motor responses (VMR1-3), acoustic startle responses (ASR1,2), acoustic startle habituation (ASH1), potentiation of habituation (ASH1/ASH5), and memory retention (ASR3/ASR2) (**Fig. 1a**). Overall, four stimulus modalities were used. This included visual light at intensities of 0 lux (dark condition) and 7.5 klux (light condition). In addition, in 5 dpf larvae responding to a 300 Hz frequency, low- (65 dB) and high-volume (75 dB) acoustic stimuli were used (**Extended data Fig. 1**) These stimuli provoked stereotyped motor activity patterns in larval zebrafish that were quantified as pixel change per second for each individual per well (**Fig. 1a**). First, in the BSL assay, zebrafish showed low average baseline activity per second. In the VSR assays, transitions from dark-to-light (**Fig. 1b**) or light-to-dark (**Fig. 1d**) conditions elicited rapid motor responses lasting 1 s. During the VMR assays, visual light caused low basal activity (**Fig. 1c**), whereas a lack of visual light gradually increased motor activity to a maximum after approximately 4 min which was followed by an asymptotic decrease to baseline (**Fig. 1e**). In the ASR1 and ASR2 assays, five low- or high-volume acoustic stimuli, with an inter-stimulus interval of 1 min, evoked weak or strong motor responses, respectively (**Fig. 1f,g**). Next, a series of 30 high-intensity acoustic stimuli with an inter-stimulus interval of 1 s induced robust habituation (**Fig. 1 h,i**). Repetitive application of habituation trials with an inter-bout interval of 1 min gradually decreased motor activity (**Fig. 1j**), indicating potentiation of habituation. Following a 3 min rest period, five high-volume acoustic stimuli elicited motor responses significantly lower than in the ASR2 assay (**Fig. 1k**), indicating memory retention. Additional data (**Extended data Fig. 2)** indicate that the phenotyping battery fulfills hallmark criteria of non-associative habituation learning[55]. Thus, we hypothesized that the VAMR battery has the potential to identify compounds that modulate visual and acoustic behaviors in larval zebrafish, including learning and memory.

## Known modulators of habituation learning alter multiple zebrafish behaviors

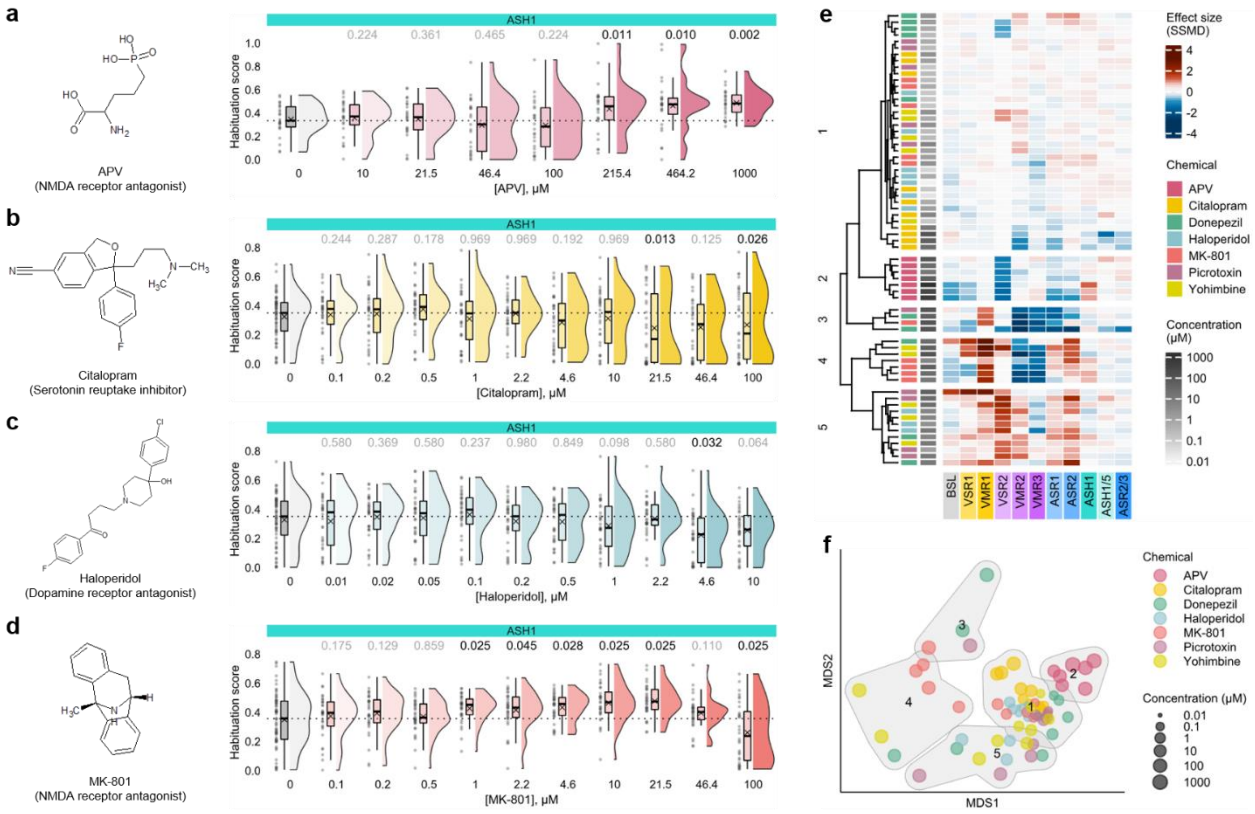


**Figure 2 | Modulators of habituation learning cause distinct behavioral phenotypes.** (**a-d**) Structures, modes of action, and habituation scores of reference modulators of habituation. Raincloud plots quantify acoustic startle habituation as habituation scores (y-axis) across indicated compounds and concentrations (x-axis). Horizontal dotted lines indicate the median habituation score of untreated larvae. Numbers above the rainclouds represent adjusted p-values (grey: $p \geq 0.05$, black: $p < 0.05$, two-sample bootstrapping test, $n_{control}$ = 24-64, $n_{treatment}$ = 24-32). Habituation scores significantly greater than negative control indicate reduced habituation whereas reduced values reflect enhanced habituation. (**e**) Hierarchical clustering of compound- and concentration-specific profiles (y-axis), across the entire assay battery (**Fig. S4**), based on effect sizes (SSMD, strictly standardized median difference) across behavioral endpoints (x-axis). Heatmap colors indicate deviation from the median control phenotype where red and blue reflect increased and reduced activity, respectively. (**f**) Multidimensional scaling (MDS) representation of pairwise distances between behavioral profiles based on data shown in **e**. Contour labels (grey) and numbers indicate clusters shown in **e**.

To evaluate the assay battery, we first tested a reference set of compounds that act through mechanisms previously reported to modulate habituation learning in zebrafish[46,47] (**Supplementary Table 3**). Selected compounds included those reported to reduce short-term habituation including two NMDAR antagonists (APV, MK-801) and donepezil (acetylcholinesterase inhibitor) and compounds that reportedly enhance short-term habituation including citalopram (selective serotonin reuptake inhibitor), haloperidol (dopamine D2 receptor antagonist), picrotoxin ($GABA_AR$ antagonist), and yohimbine (α-2 adrenoreceptor antagonist).

Larval zebrafish were exposed to a series of 7-10 concentrations per compound for 1 h before quantification of motor activity. To quantify habituation behavior, the initial habituation bout (ASH1) was used to calculate a 'habituation score,' achieved by dividing the motor activity during the final ten taps by the cumulative responses during the initial and final ten acoustic stimuli. On average, the untreated vehicle control exhibited a habituation score of 0.32. Compounds that reduced short-term habituation therefore generated values greater than the control group. In contrast, compounds that accelerated the habituation response yielded values lower than the control. In line with previous reports, the prototypical NMDAR antagonists APV and MK-801 significantly reduced non-associative habituation learning in a concentration-dependent manner (**Fig. 2a,d**), whereas citalopram (21.5, 100 µM) and haloperidol (1, 4.6 µM) significantly enhanced habituation (**Fig. 2b,c**). In addition, MK-801 significantly enhanced habituation at the highest test concentration (**Fig. 2d**). Non-significant alterations in habituation were determined in zebrafish exposed to picrotoxin, donepezil, or yohimbine (**Supplementary Fig. 1**). Together, these data suggest that the VAMR assay battery can be used to identify chemicals that modulate habituation behavior in zebrafish.

To determine whether the reference compounds selectively modulated short-term habituation learning, we simplified motor activity patterns by condensing compound- and concentration-dependent responses into behavioral profiles reflecting effect size relative to vehicle control (**Fig. 2e, Supplementary Fig. 2**). Except for habituation (described above), habituation potentiation, and memory retention endpoints, the cumulative motor activity per assay for each individual was calculated. The ‘potentiation score’ (ASH1/5) reflects the ratio of the scaled sum of motor responses during taps in the final habituation bout (ASH5) to the sum of responses in the initial (ASH1) and final (ASH5) habituation bouts. Motor activity in the ASR3 assay, relative to an individual’s overall responses summed across ASR2 and ASR3 assays, was used to quantify memory retention (ASR2/3). Subsequently, we determined effect sizes relative to vehicle control for each of the eleven endpoints, yielding compound- and concentration-specific behavioral profiles. To determine phenotypic similarities between behavioral profiles, we used two complementary approaches, hierarchical clustering (**Fig. 2e**) and multidimensional scaling (**Fig. 2f**). While the majority of compounds caused slight behavioral changes in the lower concentration range (cluster 1), exposure to higher concentrations provoked diverse multi-behavioral phenotypes (clusters 2-5) (**Fig. 2e**). Within these clusters, chemical exposure caused different combinations of behavioral alterations, such as enhanced visual and acoustic startle responses (cluster 5), hyper- and hypolocomotion in response to light or dark conditions (cluster 4), or reduced visual and acoustic startle activity (clusters 2 and 3) (**Fig. 2e**). Behavioral profiles of the

NMDAR antagonist APV (cluster 2) were segregated from all other profiles including concentrations that significantly reduced habituation (**Fig. 2e,f**). While both NMDAR antagonists (APV and MK-801) blocked habituation learning and reduced dark-to-light visual startle responses in zebrafish, disparate phenotypes were also observed. Specific to APV, exposure also reduced all other visual and acoustic startle responses (**Fig. 2e, Supplementary Fig. 2**). In contrast, MK-801 exposure enhanced acoustic startle responses, caused light-sensitive hyperlocomotion, and decreased responsiveness under dark conditions (**Fig. 2e, Supplementary Fig. 2**). At concentrations that decreased habituation, behavioral profiles of MK-801 differed from APV and clustered with profiles of picrotoxin (cluster 3), donepezil (clusters 3 and 4), and yohimbine (cluster 4) (**Fig. 2e,f**). Together with *in silico* target predictions (**Supplementary Table 4**), these data suggest that potential off-target site(s) of MK-801 in zebrafish might involve $GABA_A$ and/or acetylcholine receptors. In sum, while the assay battery illustrates a lack of selectivity for known habituation modulators, it highlights the ability to identify and discriminate chemical mode of action information.

## Targeted screen for chemical compounds that affect learning and memory identifies chlorophene

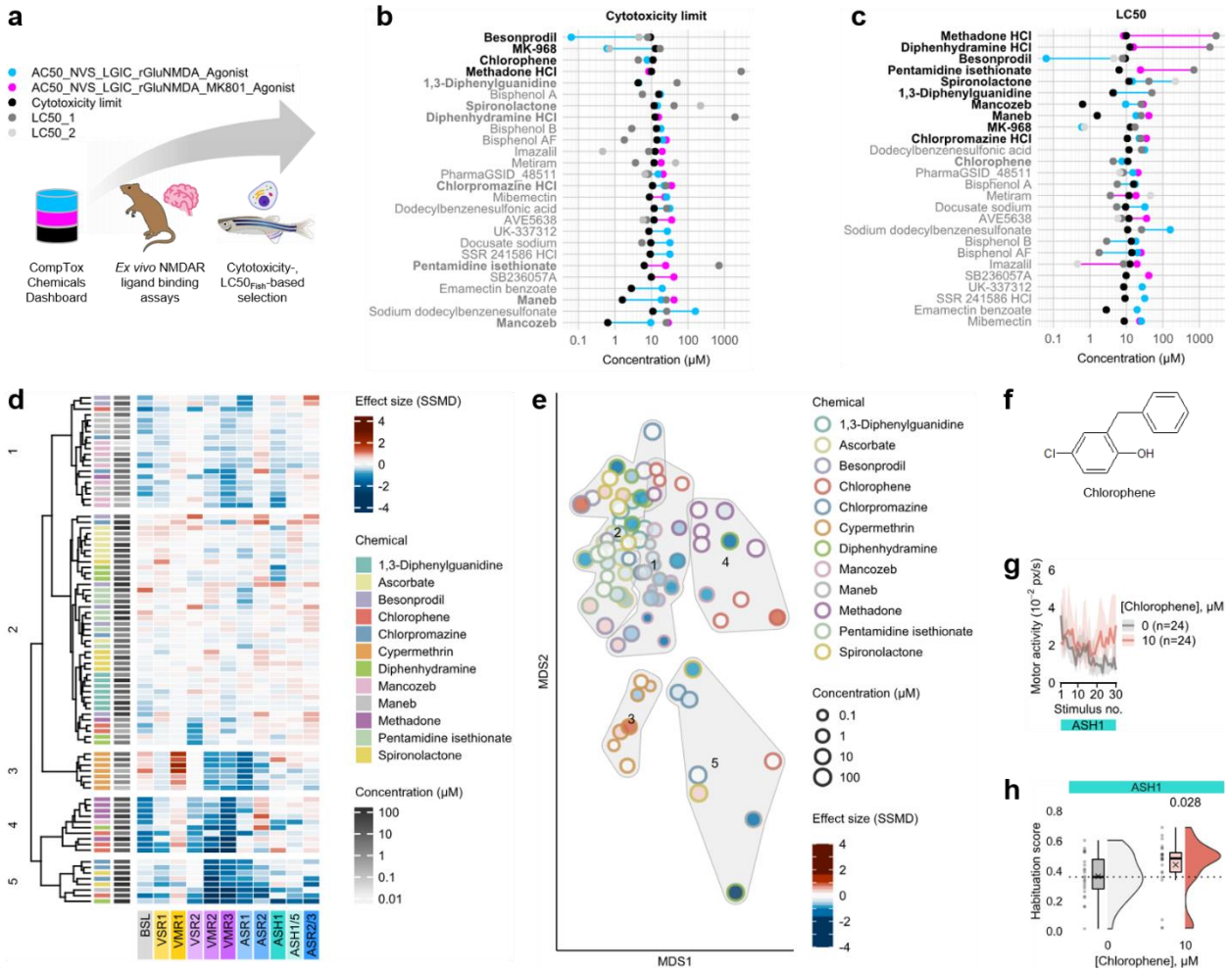


**Figure 3 | Prediction and evaluation of chemical compounds that interfere with NMDAR-dependent signaling.** (**a**) Data on *ex vivo* rat glutamate receptor radioligand binding ($AC_{50}$: blue, pink), *in vitro* cytotoxicity limit (lower bound on the estimate of the cytotoxicity threshold; black), and predicted baseline toxicity in fish ($LC_{50}$; grey) were gathered from the US EPA CompTox Chemical Dashboard and ECOSAR. (**b**) Cytotoxicity- and (**c**) baseline toxicity-based rankings of 26 *ex vivo* positive chemicals (y-axis) predict 11 unique candidate compounds (black) that alter NMDAR agonist activity with higher potency relative to cytotoxicity and predicted baseline toxicity levels. (**d**) Hierarchical clustering of behavioral profiles for 10 predicted candidate compounds and two negative reference chemicals (ascorbate, cypermethrin) (y-axis) across behavioral endpoints (x-axis). Heatmap colors based on effect sizes (SSMD, strictly standardized median difference) indicate deviation from the median control phenotype. Red and blue reflect increased and reduced activity, respectively (*n* = 12-24 larvae per condition). (**e**) MDS representation of pairwise distances between behavioral profiles based on data shown in **d**. Fill color indicates deviation from the median control phenotype in the acoustic startle habituation (ASH1) assay where red and blue reflect reduced and enhanced habituation, respectively. Contour labels (grey) and numbers indicate clusters shown in **d**. (**f**) Structure of the positive hit chlorophene. (**g**) Median motor activity (y-axis) of vehicle control (0.01% DMSO, grey) and chlorophene-exposed (10 μM, red) zebrafish larvae over 30 sequential (ISI = 1 s) high-intensity acoustic stimuli (x-axis) (shaded envelope

represents the 95% confidence interval). (**h**) Raincloud plot showing the habituation score (y-axis) for zebrafish exposed to 0.01% DMSO (vehicle control; grey) or chlorophene (10 µM, red) (horizontal dotted line; median control habituation score). The number above the raincloud represents the adjusted p-value (two-sample bootstrapping test).

Based on these results, we hypothesized that the assay battery could be used to identify chemical compounds that affect learning and memory in zebrafish. Given the well-characterized involvement of NMDARs in synaptic plasticity and memory function[56–58], we conducted a targeted selection of candidate compounds. The EPA CompTox Chemicals Dashboard, which contains bioactivity data on thousands of chemicals tested across numerous high-throughput screening assays[59], was mined for relevant assays. We identified two tissue-based, cell-free radioligand binding assays that used extracted proteins from rat forebrain membranes to determine changes in NMDAR agonist activity (**Fig. 3a**, **Supplementary Table 5**). In total, these datasets contained 81 unique chemicals of which 26 were annotated as hits (**Supplementary Table 6**). To enrich the set of hits for compounds that exhibited higher specificity towards NMDARs relative to non-specific general toxicity, we used *in vitro* cytotoxicity and baseline toxicity data (**Supplementary Table 7**). These data were used to rank order compounds according to their specificity for NMDAR interaction relative to non-specific toxicity effects (**Fig. 3a-c**). Rankings predicted 11 compounds with higher potency for NMDAR modulation relative to cytotoxicity and baseline toxicity levels (**Fig. 3b,c**). For example, besonprodil and MK-968, two preclinical drugs that act as NMDAR antagonists, and methadone, a µ-opioid receptor antagonist used as a painkiller, were among the predicted hits that appeared in both rankings (**Fig. 3b,c**). Ten compounds were purchased and screened in our behavior assay battery. In addition, we selected two chemicals (cypermethrin, ascorbic acid) as negative reference compounds for NMDAR modulation. Cypermethrin is a pyrethroid insecticide that prolongs the opening of sodium channels[60]. From a structural perspective, it is closely related to deltamethrin, a developmental neurotoxicant[61]. In contrast, ascorbic acid was proposed as a negative chemical for developmental neurotoxicity[25].

To determine whether exposure to the selected compounds affected behavior, we treated zebrafish for 1 h with multiple concentrations of each test chemical and translated the 11 quantitative features into behavioral profiles (**Supplementary Figure 3**). Hierarchical clustering segregated compound- and concentration-dependent profiles into five main clusters (**Fig. 3d**). Cluster 1 was characterized by decreased activity in multiple visual and acoustic startle response assays and contained compounds such as chlorpromazine (neuroepileptic) and spironolactone (diuretic) (**Fig. 3d**). A second cluster (cluster 2), characterized by enhanced responsiveness to high-volume acoustic stimuli, included diphenhydramine (antihistamine) and methadone (**Fig. 3d**). Cluster 3 exclusively contained cypermethrin which provoked light-sensitive hyperlocomotion in a

concentration-dependent manner and decreased motor activity across multiple visual- and acoustic-based endpoints (**Fig. 3d**). To visualize chemical modulators of habituation learning among the variety of phenotypes, we projected all multi-behavioral profiles into two dimensions using multidimensional scaling and shaded each data point with the effect size determined in the ASH1 assay (**Fig. 3e**). We found that behavioral profiles with enhanced or reduced startle habituation spread across the two-dimensional space, reflecting diverse multi-behavioral phenotypes (**Fig. 3e**). Diphenhydramine (1, 4.6-100 µM), the structurally related fungicides mancozeb (0.1-4.6 µM) and maneb (0.1-21.5 µM), and spironolactone (46.4 µM) significantly enhanced acoustic startle habituation (**Fig. 3e**, **Supplementary Fig. 4**, $p < 0.05$, two-sample bootstrapping test). Three compounds including besonprodil (100 µM, cluster 2), cypermethrin (10 µM, cluster 3), and chlorophene (10 µM, cluster 4), reduced acoustic startle habituation (**Fig. 3d**), although only the habituation decrease caused by chlorophene was statistically significant (**Fig. 3f-h**, **Supplementary Fig. 4**, $p = 0.028$, two-sample bootstrapping test). Overall, half (5/10) of the predicted hits were active in our ASH1 assay. Surprisingly, while one of the negative reference chemicals, cypermethrin, was indeed inactive, ascorbate (10-21.5 µM, 100 µM) significantly enhanced acoustic startle habituation (**Supplementary Fig. 4**). Together, these data suggest that the VAMR behavior assay battery is useful for identifying compounds that also modulate NMDAR-mediated signaling in rat *ex vivo* preparations. In addition, relative to *in vitro* or *ex vivo* biochemical assays, and based on the diversity of potential phenotypic outcomes, the zebrafish assay has the potential to elucidate additional, previously unknown phenotypes that can be mechanistically evaluated.

## Chlorophene does not directly act on NMDARs and alters neuronal firing

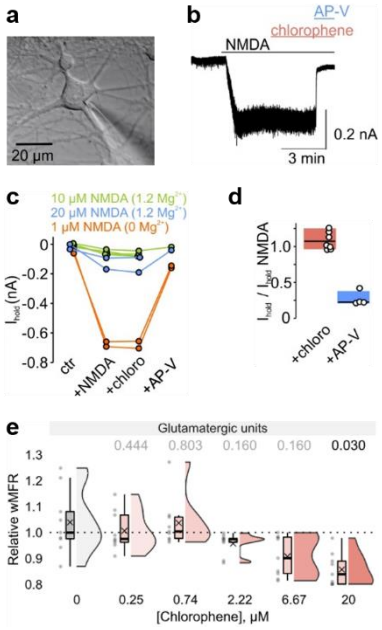


**Figure 4 | Chlorophene does not act on NMDARs in cultured mouse cortical neurons but reduces the weighted mean firing rate of glutamatergic units in human stem cell-derived 3D BrainSpheres.** (**a**) Representative infrared differential interference contrast image of a patch-clamped cultured mouse cortical neuron. (**b**) Representative current response to NMDA (1 µM) remained unchanged during chlorophene (10 µM) application, but was inhibited by the NMDAR antagonist APV (50 µM). (**c**) Individual holding currents ($I_{hold}$) before (ctr) and during NMDA administration were not affected by chlorophene (+chloro, $n$ = 8), but inhibited by APV ($n$ = 4). (**d**) Relative $I_{hold}$ during chlorophene (n=8) and APV (n=4) application compared to $I_{hold}$ evoked by respective NMDA exposure. (**e**) Weighted mean firing rate (y-axis) of human stem cell-derived 3D-differentiated BrainSpheres exposed to increasing concentrations of chlorophene (x-axis). After the first baseline recording, the neurotransmitter glutamate, followed by the antagonists APV/NBQX, were applied to identify glutamatergic units (two-sample bootstrapping test, $n$ = 9).

Given its wide use as a biocide, preservative, and disinfectant[62,63], we investigated chlorophene in more detail. Because chlorophene exposure impaired habituation in zebrafish (**Fig. 3g,h**), altered NMDAR agonist activity in rat *ex vivo* preparations (**Fig. 3b**), and given the crucial role of NMDARs in neuroplasticity, we hypothesized that chlorophene reduced habituation learning by targeting NMDARs. We further hypothesized that the underlying molecular mechanisms may also be conserved across taxa, including mice and humans. To evaluate the translational relevance of these findings, we used whole-cell patch-clamp recordings in cultured mouse cortical neurons (**Fig. 4a**). We found that, while the NMDAR antagonist APV effectively inhibited the current response provoked by NMDA application, chlorophene application failed to do so (**Fig. 4b-d**). As a second approach to determine whether chlorophene targeted glutamatergic signaling, the compound was evaluated in a microelectrode array (MEA) assay using human-induced pluripotent stem cell-derived (hiPSC) 3D BrainSpheres. In this *in vitro* model, chlorophene exposure reduced

the weighted mean firing rate of glutamatergic units in a concentration-dependent manner (**Fig. 4e**). Together, although chlorophene may interact with glutamatergic signaling, these data do not support the hypothesis that chlorophene directly antagonizes NMDARs leading to reduced habituation in zebrafish.

## Chlorophene acts on GABAARs in zebrafish, mouse, and human models

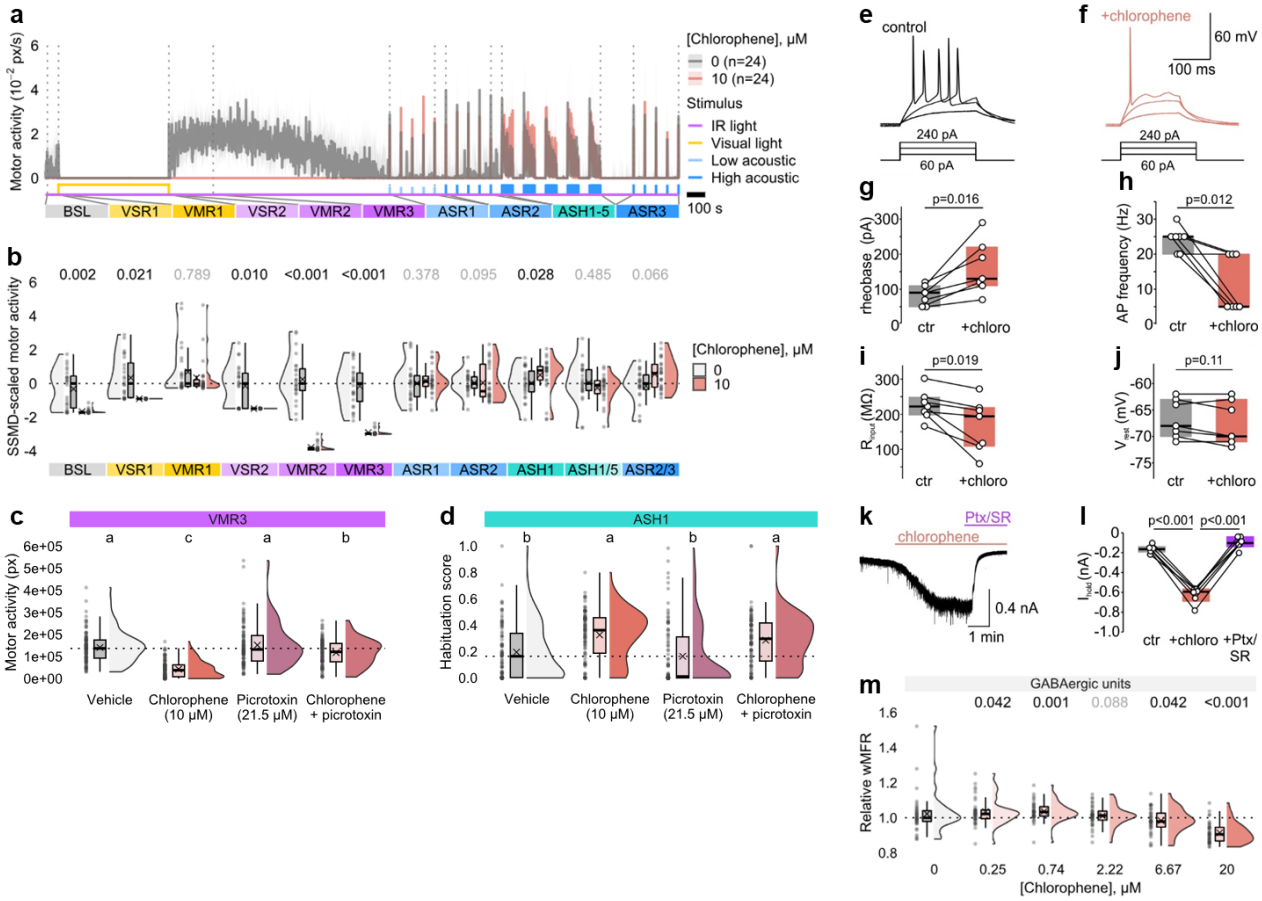


**Figure 5 | Chlorophene affects GABAergic signaling in zebrafish, cultured mouse cortical neurons, and human stem cell-derived 3D BrainSpheres.** (**a**) Motor activity (y-axis) of zebrafish treated with chlorophene (10 µM, red) or 0.01% DMSO (grey) over time and across various stimulus modalities (x-axis). Data represents median ± 95% CI. (**b**) Split raincloud plots show the effect of chlorophene exposure on zebrafish motor activity (y-axis) across 11 assay endpoints (x-axis). Motor activity is expressed as effect size (SSMD, strictly standardized median difference) to represent different assay endpoints on a common scale. Data points are equally shifted to set the median control activity per assay endpoint to zero. Numbers above the rainclouds represent adjusted p-values (grey: $p \geq 0.05$, black: $p < 0.05$, two-sample bootstrapping test). (**c**) Representative raincloud plot showing the cumulative motor activity (y-axis) of zebrafish exposed to the indicated compounds (x-axis) in response to dark conditions (VMR3) (Kruskal-Wallis test, $n$ = 94-96 larvae). (**d**) Habituation scores (y-axis) of zebrafish treated with the indicated compounds (x-axis). A sequence of 30 high-intensity acoustic stimuli with 1 s ISI was used to induce acoustic startle habituation (ASH1) (Kruskal-Wallis test, $n$ = 94-96 larvae). (**e**) Representative response of a cultured mouse cortical neuron to depolarizing current injections under the control condition (black) and (**f**) during chlorophene application (10 µM, red). (**g-j**) Passive

membrane and intrinsic properties of cultured mouse cortical neurons without and during application of chlorophene including (**g**) rheobase, (**h**) action potential (AP) firing frequency at 2x rheobase, (**i**) input resistance ($R_{input}$), and (**j**) resting membrane potential ($V_{rest}$) (paired t-tests, n=7). (**k**) Representative current response of a cultured mouse cortical neuron to chlorophene (10 µM) was inhibited by co-exposure to the $GABA_A$ receptor antagonists picrotoxin (Ptx, 50 µM) and SR95531 (SR, 10 µM). (**l**) Individual and median holding current ($I_{hold}$) under control condition, during chlorophene application and $GABA_A$ receptor blockade by picrotoxin and SR95531 (repeated measures ANOVA, Bonferroni t-test, *n* = 6). (**m**) Weighted mean firing rate (y-axis) of 3D BrainSpheres treated with increasing concentrations of chlorophene (x-axis). After the first baseline recording, the neurotransmitter GABA followed by the antagonist bicuculline were applied to identify GABAergic units (two-sample bootstrapping test, *n* = 46).

To determine whether chlorophene acted on targets other than NMDARs, we used the Similarity Ensemble Approach[64] to predict protein targets based on structural similarity to their ligands. Among 107 predicted targets were three $GABA_AR$ subunits including α2, α3, and α5 (**Supplementary Table 8**). Certain agonists and positive allosteric modulators of $GABA_ARs$ have been reported to cause sedation and paradoxical excitation in zebrafish[51], two phenotypes observed in chlorophene-exposed larvae (**Fig. 3g,h and Fig. 5a,b**). We therefore hypothesized that sedation in visually-mediated responses and increased responsiveness to repeated acoustic stimuli, were related to a GABAergic mode of action in chlorophene-exposed zebrafish. To determine whether chlorophene exposure caused these phenomena via $GABA_AR$ agonism, we pretreated zebrafish with the $GABA_AR$ antagonist picrotoxin (**Fig. 5c**). Pharmacological intervention rescued chlorophene-induced sedation, restoring visual motor responses (**Fig. 5c**, **Supplementary Fig. 5**) whereas picrotoxin pretreatment did not counteract the habituation deficit caused by chlorophene exposure (**Fig. 5d**). Together, these observations suggest that exposure to chlorophene caused sedation and paradoxical excitation, but not defective habituation, through $GABA_ARs$ in zebrafish.

We next sought to evaluate whether chlorophene acts as a $GABA_AR$ agonist in mouse- and human-based models. To determine whether chlorophene acts on $GABA_A$ receptors we first measured currents in cultured mouse cortical neurons. Chlorophene exposure induced a slow tonic chloride current that was blocked by the $GABA_AR$ antagonists picrotoxin and SR95531 (**Fig. 5k,l**). This suggests that chlorophene activates rodent $GABA_ARs$. To investigate the effect of $GABA_AR$ activation by chlorophene on neuronal action potential firing, we measured the membrane potential during current injections while blocking glutamatergic receptors with APV and NBQX (**Fig. 5e-f**). Chlorophene exposure increased the minimum current needed to generate an action potential (i.e. the rheobase; **Fig. 5g**), decreased the action potential firing frequency and the input resistance (**Fig. 5h and i**), and did not change the resting membrane potential (**Fig. 5j**). These data suggest that chlorophene-induced $GABA_AR$-mediated chloride conductance shunts

neuronal action potential spiking by lowering the input resistance and increasing the current threshold required for neuronal spiking. To determine whether chlorophene acts as a $GABA_AR$ modulator in humans, we used the 3D BrainSphere MEA assay where the weighted mean firing rate of GABAergic units was significantly decreased in chlorophene-treated (6.7-20 µM) 3D BrainSpheres (**Fig. 5m**). In summary, these data indicate that chlorophene likely acts through similar mechanisms in zebrafish, mouse, and human-based models to agonize $GABA_ARs$.

## Discussion

Given the ubiquitous exposure to diverse environmental chemicals across lifespan and the vast dearth of information on the hazards presented by these chemical compounds, there is an unmet need to efficiently assess their potential adverse effects on neurodevelopment and function. Here we describe a multi-behavioral phenotyping approach in early life-stage zebrafish that enables (i) the rapid identification of neuroactive compounds and (ii) the elucidation of mechanisms underlying alterations in neurobehavior. While current behavior-based toxicity tests in larval zebrafish, such as the light-dark transition test[65–68], largely focus on a small number of visual motor behaviors, we merged this widely used assay with additional, well-described paradigms, broadly applied in large-scale behavioral drug screens, including acoustic startle responses[48,51], habituation learning[46,47,49], and other memory-related endpoints that have yet to be applied to toxicity testing.

This work focused on the identification of chemical modulators of habituation, which is a form of non-associative learning[55]. Defective habituation is associated with decrements in learning and memory[69,70] and is prevalent in neuropsychiatric disorders such as autism spectrum disorder, schizophrenia, and attention deficit hyperactivity disorder[71]. Here, we demonstrated that the phenotyping battery fulfills hallmark criteria of non-associative learning[55], a phenomenon conserved across phyla including zebrafish[47], rodents[72], and humans[73]. Confirmation of habituation characteristics (**Extended Data Fig. 2**) and the reproducibility of phenotypes observed with known habituation modulators demonstrate that the VAMR battery quantifies non-associative learning. This includes a quantitative demonstration of dishabituation, which is defined as an increased response to a habituated stimulus following a second, brief stimulus using a different stimulus modality[55]. Dishabituation to acoustic stimuli has been quantitatively demonstrated 7 dpf zebrafish using a second, light-based stimulus[47] while in 6 dpf larvae, dishabituation following a user-based tactile stimulus has been reported[46,74]. This study demonstrates dishabituation in 5 dpf zebrafish, using a light-based secondary stimulus and thereby avoiding the use of a tactile stimulus which could cause confounding effects on swimming behavior (**Extended Data Fig. 2**).

In line with previous studies, we found that acute administration of the prototypical NMDAR antagonists APV or MK-801 reduced acoustic startle habituation in zebrafish[46,75]. This observation is consistent with deficits in learning and memory reported in rodent-based test paradigms[76,77]. We found a lack of selectivity for habituation with different chemical modulators. This may result from off-target activities or systemic compound interactions across multiple molecular targets that orchestrate behavior. The mode(s) of action underlying behavioral alterations in zebrafish exposed to MK-801 for example, are not completely understood. *grin1* encodes the obligatory

GluN1 subunit of NMDARs[78]. While behavioral defects in *grin1* double mutants are generally phenocopied by short-term MK-801 treatment[79], off-target activities on acetylcholine receptors[80] and voltage-gated potassium channels[81] may explain the difference in phenotypes observed in zebrafish exposed to MK-801 and APV. Overall, our data indicate that zebrafish multi-behavioral phenotyping strategies can be used to identify complex, system-modulating compounds.

We found that exposure to chlorophene, a chlorinated phenolic compound, caused reduced habituation learning, sedation, and paradoxical excitation in zebrafish. Sedatives and general anesthetics (e.g. benzodiazepines, propofol, etomidate) can cause paradoxical excitation where an opposite, paradoxical reaction induces both sedation and increased brain and/or motor activity[82–84]. It is widely accepted that anesthetics induce neuronal suppression via GABAR agonism, NMDAR antagonism, or by membrane polarity modulation[85–89]. Several lines of evidence indicate that chlorophene also acts on $GABA_A$Rs. First, among other proteins, SEA algorithms[64] predicted multiple $GABA_A$R subunits to be targeted chlorophene, including subunits α2, α3, and α5. Second, chemical intervention using the $GABA_A$R antagonist picrotoxin counteracted sedation of visual motor behaviors in zebrafish. Third, tonic inhibition against neuronal excitability in cultured mouse cortical neurons was blocked by the $GABA_A$R antagonists picrotoxin and SR95531. Fourth, chlorophene exposure reduced the weighted mean firing rate of GABAergic units in hiPSC-derived 3D BrainSpheres.

Most $GABA_A$R α subunits are expressed during zebrafish embryogenesis[90]. The amino acid sequences and electrophysiological properties of $GABA_A$R subunits are largely conserved among vertebrates including zebrafish, mice, and humans[91]. Several studies suggest that α5-$GABA_A$R-mediated tonic inhibition reduces learning and memory[92–98]. Under physiological conditions, tonic $GABA_A$R currents cause hyperpolarization and decrease neuronal excitability. Synaptic input, therefore, becomes subthreshold and interferes with coordinated pre- and post-synaptic spiking activity, which is required for NMDA-dependent long-term plasticity[99]. Antagonizing GABAergic tone facilitates neuroplasticity in genetic mouse models for cognitive disabilities[100,101]. In contrast, the deficits in learning and memory in zebrafish described here were not rescued by the $GABA_A$R antagonist picrotoxin. Our results indicate that reduced habituation may result from a mechanism distinct from functional $GABA_A$R agonism. Alternatively, co-occurring phenotypes including sedation, paradoxical excitation, and defective learning, may causally relate to a common, unknown upstream regulator.

NMDARs are essential to mediate experience-dependent neuroplasticity underlying learning and memory[58,78]. In teleost fish, including zebrafish, the telencephalon, and in particular the medial

and lateral pallium, are analogous to amygdala and hippocampus in mammals[102–104] and represent the neuroanatomical structures responsible for learning and memory involving NMDAR activation[105–107]. However, our electrophysiological data indicates that chlorophene does not directly interfere with NMDAR-dependent signaling in mouse cortical neurons. This suggests that chlorophene indirectly affects NMDARs, phenocopying the decreased habituation observed in zebrafish exposed to NAMDAR antagonists. A large-scale screen for chemical modulators of non-associative learning identified additional mechanisms reducing short-term habituation in larval zebrafish including potassium channel antagonism[46]. Interestingly, another zebrafish-based small molecule screen implicated that the M-current, a voltage-gated potassium channel that regulates neuronal excitability[108], is related to sedation and paradoxical excitation[51]. Our screen confirmed that exposure to diphenhydramine, an antihistamine used in some hypnotic preparations, caused sedation and paradoxical excitation in early life stage zebrafish[109]. Surprisingly, as compared to chlorophene, diphenhydramine exposure had the opposite effect on non-associative learning, enhancing short-term habituation in zebrafish. Future studies should investigate whether M-current modulators counteract the sedative, paradoxical excitatory, and habituative learning effects of compounds such as chlorophene and diphenhydramine.

Chlorophene and its structural analogues, known as chlorophenes, represent a group of halogenated phenolic compounds that are globally used as antimicrobial agents and preservatives in personal care products and cosmetics[63,110]. Their environmental occurrence in surface waters and soils exclusively results from anthropogenic activities through emissions from sewage treatment plants and application of sewage sludge[110–112]. Based on a predicted environmental concentration (PEC) of 0.2 µg/L (0.9 nM) and a predicted no effect concentration (PNEC) of 0.058 µg/L (0.3 nM), a risk quotient (RQ=PEC/PNEC) of 3.4 has been calculated for the emission of chlorophene into surface waters, indicating that chlorophene may pose an unreasonable risk to the aquatic environment[110,113]. Consequently, chlorophene is included on international lists of environmental chemicals of emerging concern[110]. This, paired with the toxicity data reported here, suggests that (bio)monitoring in human and environmental matrices is justified.

Chlorophenes are hydrophobic (log $K_{OW}$ 4.3-7.5), persistent (ultimate biodegradation half-life 1.9-4.9 years), low-to-moderately bioaccumulative in fish (BCF 55-400 L/kg), and toxic to aquatic organisms including fish, invertebrates, and algae[110,113]. In particular, chlorophene's 30-day no observed effect concentration ($NOEC_{chronic}$) for survival in zebrafish (Fish Early Life Stage Test, OECD TG 210[114]) of 0.58 mg/L (2.7 nM) indicates high chronic toxicity (acute-to-chronic ratio; ACR=$LC50_{acute}/NOEC_{chronic}$=569) and is consistent with a specific mode of action[62,110,113,115]. Our study suggests that chlorophene acts as a functional agonist at $GABA_A$Rs, indicating a neurotoxic

mode of action. Currently, adult or developmental neurotoxicity assessment is addressed under the Classification, Labeling and Packaging (CLP) Regulation[116,117], REACH (Registration, Evaluation, Authorisation and Restriction of Chemicals), and the Biocidal Products Regulation (BPR). Under CLP, developmental neurotoxicity studies are required if there is evidence that the nervous system is a target organ including any effect interfering with normal development until sexual maturation, including death, structural abnormality, altered growth, and functional deficits[118], whereas both under REACH and BPR, adult neurotoxicity (functional or morphological alterations in the mature nervous system) triggers tests on developmental neurotoxicity[119,120]. Interestingly, an ECHA (European Chemicals Agency) assessment reports state that chlorophene has "…no structural similarity to […] known inducers of delayed neurotoxicity" and that "[…] studies in several species did not reveal the potential for neurotoxic effects […]"[62]. This discrepancy underscores limitations in current neurotoxicity assessment practices as this conclusion was reached without conducting regulatory adult or developmental neurotoxicity tests.

In addition to neurotoxicity, there is increasing evidence that chlorophene and related chemical compounds act as endocrine-disrupting chemicals (EDCs) that interfere with hormonal homeostasis. In cell-based luciferase reporter assays *in vitro*, chlorophene modulated androgen, estrogen, and thyroid receptor activity, and meets the criteria for an EDC[121]. A structurally related compound, bromochlorophene, was shown to act as an antagonist on androgen, estrogen, glucocorticoid, and thyroid receptors *in vitro*[121]. Given that GABA is widely distributed in endocrine tissues and serves as a hormone or trophic factor in neuroendocrine systems[122,123], and considering that changes in hypothalamic GABA levels are involved in endocrine disorders[124,125], a potential link between altered GABAergic signaling and endocrine disruption should be addressed in EDC-related studies.

In the future, zebrafish multi-behavioral assays might be utilized for the regulatory assessment of chemical-induced neurotoxicity. The European Union's chemicals strategy (European Green Deal) aims to enhance innovation for safe and sustainable chemicals to better protect human health and the environment[126]. To improve public health and environmental protection under legislative instruments such as REACH and CLP, current risk assessment should prevent the use of chemicals that affect neurological systems[126]. Because current regulatory DNT testing is exclusively conducted in rodents (e.g., OECD Test No. 426: Developmental Neurotoxicity Study[27]), less than 0.06% of an estimated 350,000 commercially available chemicals[2] have been evaluated for potential effects on the developing nervous system[25]. As a result, there is an urgent need for alternative, rapid, inexpensive, and 3R-compliant[38] approaches to evaluate potential DNT effects. Compared to cell-based *in vitro* neurotoxicity methods[127,128], multi-behavioral phenotyping

in zebrafish represents a more holistic and untargeted approach to identify neurotoxicants and to infer their potential chemical mode(s) of action. In addition, unlike *in vitro*-based approaches, early life-stage zebrafish capture the functional complexity of the vertebrate nervous system[129], including its conserved developmental biology that is relevant to higher vertebrates including humans[130]. In addition, zebrafish are metabolically competent, enabling the identification and characterization of adverse effects derived from biotransformation products[131,132]. While the zebrafish phenotyping battery contains multiple learning- and memory-related readouts including habituation, potentiation of habituation[46], and memory retention[46,75] that serve as potential correlates to behavior-based endpoints in OECD rodent neurotoxicity test guidelines[27], more work is needed to understand the direct relationship between rodent- and zebrafish-based behavior readouts.

In summary, we combined a series of behavior assays in a non-mammalian vertebrate model to screen chemicals for neurotoxicity in a phenotypically rich, rapid, and inexpensive test system. Together with *in silico* target predictions, and mouse- and human-based models, our findings establish multi-behavioral phenotyping as a powerful toolkit for neurotoxicity testing and mechanism identification, with cross-species relevance. More broadly, multi-behavioral phenotyping in zebrafish can accelerate the identification of neuroactive chemicals that should be prioritized for additional testing to better protect human health and the environment from chemicals that disrupt nervous system function.

## Methods

### Zebrafish maintenance and embryo collection

All protocols and procedures involving zebrafish were conducted according to German and European animal protection standards and were approved by the Government of Saxony (Landesdirektion Leipzig, file number 75-9185.64). Adult zebrafish (*Danio rerio*), derived from an outcross of WIK and an in-house 'UFZ-OBI' strain, were maintained on a 14-h light, 10-h dark cycle at 28 °C and fed twice a day during the week and once daily on weekends with live brine shrimp and/or SDS 400 dry feed (Special Diets Services). Fertilized eggs were collected from group breeds containing 120-140 fish/120 L water and were bleached for 5 min with 0.05% NaOCl at 3-4 h post-fertilization (hpf). Embryos were raised in crystallization dishes at a density of 50 embryos per 100 mL standard dilution water (ISO 7346-3; 80 mM $CaCl_2 \cdot 2H_2O$, 20 mM $MgSO_4 \cdot 7H_2O$, 31 mM $NaHCO_3$, 3.1 mM KCl, pH 7.4) until 4 dpf. Viable, hatched, and morphologically normal larvae with an inflated posterior swim bladder were individually distributed into single wells of clear polystyrene flat-bottom 96-square-well plates (Cytiva, Marlborough, MA,

USA) filled with 200 µL standard dilution water. Plates were covered with microseal 'A' film (Bio-Rad Laboratories, Hercules, CA, USA) and microplate lids (Cytiva, Marlborough, MA, USA). Plates were stored at 28 °C on a 14-h light to 10-h dark cycle prior chemical exposure at 5 dpf.

**Zebrafish chemical exposure**

Chemical compounds are listed in **Supplementary Table 1**. Pharmacological modulators of habituation learning, selected based on previous studies in larval zebrafish (**Supplementary Table 3**), were dissolved in standard dilution water. Environmentally-relevant chemical compounds, selected from *ex vivo* studies, were dissolved in dimethyl sulfoxide (DMSO, Merck, 1.02952.1000, ≥99.9% purity). 100 mM chemical stock aliquots, prepared in DMSO, were stored at -80 °C. Serial dilutions were prepared from 200 µM chemical stock solutions adjusted to pH 7.4. At 5 dpf, larvae were exposed to 200 µL of 2× exposure solutions for a final volume of 400 µL per well. Each compound was tested at 7-10 concentrations that ranged from 0.1-100 µM, unless otherwise indicated. When DMSO was used, the control group was exposed to an equal volume for a final concentration of 0.01% DMSO. Compounds were tested in 8-24 replicate wells across 2-4 replicate plates using larvae from two independent spawning events. To detect acute, receptor-mediated effects, larvae were exposed for 40 min (28 °C, light on) prior to behavior analysis. For behavior phenotype rescue experiments, larvae in 200 µL standard dilution water were pre-treated with 100 µL 3× picrotoxin solution at a concentration of 64.6 µM (21.5 µM final concentration) or vehicle for 15 min, followed by addition of either 100 µL 4× chlorophene solution at 27.3 µM (6.8 µM final concentration), 21.5 µM picrotoxin, a mixture of chlorophene and picrotoxin (6.8 µM chlorophene, 21.5 µM picrotoxin final concentration), or vehicle. The final concentration of DMSO was 0.01% for all groups. Plates were incubated for an additional 25 min before behavior acquisition.

**Zebrafish automated behavior assay battery and motor activity quantification**

96-square well plates containing a single 5 dpf larva per well were loaded into a ZebraBox behavior apparatus (ViewPoint) and the measurement was initiated. The assay commenced with an initial 21 min acclimation period (1 min 100% light, 20 min 0% light). The temperature was maintained at 28°C for the duration of the experiment. Videos were recorded at 25 frames per second and ZebraLab video tracking software (ViewPoint) in 'quantization mode' (sensitivity threshold = 15) to quantify locomotor activity using pixel intensity changes per second for each of the 96 evenly-spaced, well-specific regions. In a battery of 11 behavioral assays, sequential variations in stimulus modalities (**Supplementary Table 2**) were applied to stimulate changes in locomotor activity, that were optimized considering visual (light- and dark-cycle durations) and

acoustic stimulus parameters (sound frequency, volume, inter-stimulus interval (ISI), inter-bout interval), and developmental stage (**Extended Data Fig. 1** and **2**). Infrared light was used to continuously illuminate the measuring chamber and visual light at 100% nominal intensity was determined to be 7.5 klux (LI-250 light meter, LI-COR). Acoustic stimuli with a frequency of 300 Hz were applied at nominal volumes of 75% (65 dB for ASR1) and 100% (75 dB for ASR2, ASR3, ASH1-5).

Motor activity data (Δpixel/second/well) was analyzed using custom KNIME (version 4.1.4, KNIME AG, www.knime.com) workflows implemented with R scripts[133] for statistical analysis and data visualization using the add-on packages ggplot2[134], RColorBrewer[135], and ComplexHeatmap[136]. To quantify motor activity, cumulative pixel intensity changes per second were calculated per well for each assay. The average motor activity per second during the final minute of the acclimation period was used to quantify baseline activity (assay BSL). Motor activity following dark-to-light transitions was divided into two periods reflecting rapid visual startle responses lasting 1 s (assay VSR1) and low basal activity in the following 9:59 min (assay VMR1). Subsequent changes in motor activity following light-to-dark transitions were binned into three periods including a one-second visual startle response (assay VSR2), a gradual increase in motor activity in the following 3:59 min (assay VMR2), and a transient decrease in motor activity to baseline level within the subsequent 16 min of the dark period (assay VMR3). Then, acoustic startle responses to five low-intensity (assay ASR1) and high-intensity (assay ASR2) 1-s acoustic stimuli, separated by 1-min ISIs, were averaged across five trials. Motor responses to 30 high-intensity acoustic stimuli (1-s with 1-s ISI) were condensed into a single metric reflecting acoustic startle habituation (assay ASH1) comprising the cumulative motor activity during the final ten taps scaled to the overall activity during the initial and final ten taps to account for individual differences in baseline startle activity[137]. Out of five repetitive habituation bouts with an inter-bout interval of 1 min, the ratio of motor activity during taps in the final bout (ASH5) relative to the sum of activities in the initial (ASH1) and final bout (ASH5) was calculated to quantify potentiation of habituation (ASH1/5). Habituation trials were followed by a three-minute rest period. Then, five high-intensity acoustic stimuli (1-s, 1-min ISI; ASR3) that were averaged across trials and scaled to the overall responses summed across ASR2 and ASR3 assays to quantify memory retention (ASR2/3). Following each experiment, dead larvae, identified upon visual inspection, were excluded from behavior data analyses.

**Statistics, behavioral profiling, hierarchical clustering, and multidimensional scaling for zebrafish behavior data**

Statistical analyses were performed on 11 behavior metrics including baseline activity (BSL), visual startle responses (VSR1 and VSR2), visual motor responses (VMR1-VMR3), acoustic startle responses (ASR1 and ASR2), acoustic startle habituation (ASH1), potentiation of habituation (ASH1/5), and memory retention (ASR2/3). Given the diverse, mostly nonparametric probability distributions of data across different behavior metrics, we chose a universally applicable, nonparametric bootstrapping method that is not limited by a model assumption[138]. First, the absolute value (two-sided test) of the difference in medians between untreated control and each treatment was calculated as a test statistic. Then, a *N* (number of observations to sample) times *B* (number of bootstrap samples; set to 10,000) matrix was created, where each column represented a bootstrap resample (with replacement) of the observed data. Third, the bootstrap test statistic (absolute value of the difference in medians) was calculated for each bootstrap resample per column, considering the number of observations per group. Finally, the p-value was calculated reflecting the proportion of bootstrap test statistics that were equal or greater than the observed test statistic[139,140]. For multiple comparisons, the Kruskal-Wallis rank sum test was used and the R package "agricolae"[141] was used to report results of all pairwise comparisons using compact letter displays. A Benjamini-Hochberg correction was used to adjust for multiple comparisons in order to control for family-wise Type I error rates. Results were considered significant if $p_{adjusted}<0.05$. To calculate 95% confidence intervals of the median for each one-second time bin, 1,000 bootstraps (with replacement) were sampled from the observed data and the percentile method was used to determine the lower (2.5$^{th}$ percentile) and upper (97.5$^{th}$ percentile) confidence interval bounds[142]. As a measure of effect size, strictly standardized median difference (SSMD) values were calculated as follows: $SSMD=\tilde{x}_{treatment}-\tilde{x}_{control}/(MAD^2_{treatment} + MAD^2_{control})^{1/2}$, where $\tilde{x}$ and MAD represent median and median absolute deviation[143]. SSMD calculations were performed on each of the 11 behavior metrics, collectively representing a compound's behavioral profile at a given concentration. Hierarchical clustering was performed on behavioral profiles using k-means clustering in the R package ComplexHeatmap[136]. For multidimensional scaling (MDS), two-dimensional coordinates for each behavioral profile were calculated using the KNIME nodes 'Numeric Distances' (Euclidean distance configuration), 'Distance Matrix Calculate', and 'MDS (DistMatrix)'.

**Identification of candidate compounds for zebrafish behavior-based screening**

The U.S. Environmental Protection Agency (US EPA) CompTox Chemicals Dashboard (https://comptox.epa.gov/dashboard/) was searched for assay endpoint names and genes using

the search term “NMDA”. Two assays were identified, including “NVS_LGIC_rGluNMDA_Agonist” and “NVS_LGIC_rGluNMDA_MK801_Agonist”, both representing tissue-based, cell-free radioligand binding assays on extracted gene-proteins from rat forebrain membranes relating to the gene *grin1*. Detailed assay information can be found in **Supplementary Table 5**. Among 81 unique chemical compounds present in at least one of the two datasets, 26 compounds were annotated as hits (**Supplementary Table 6**). Positive hits were included in the zebrafish behavior screen if their $AC_{50}$ (active concentration causing 50% loss in scintillation count) values were below the lower bound of cytotoxicity[144] or the predicted 96-h $LC_{50}$ in fish (ECOSAR v2.0, U.S. EPA) (**Supplementary Table 7**). Additionally, two compounds annotated as inactive, including cypermethrin and ascorbate, were selected as negative reference compounds. Chemical exposures were performed as described above.

**Molecular target prediction**

The Similarity Ensemble Approach (SEA[64]) was used to predict molecular target sites for MK-801 (**Supplementary Table 4**) and chlorophene (**Supplementary Table 8**).

**Mouse cortical cultures**

Neocortical neuronal cultures from P0 to P1 mice were prepared as previously described[145]. Briefly, mice were decapitated and cerebral cortices were removed, dissected and enzymatically digested with papain (Sigma, CAS 9001-73-4) or trypsine (Sigma, CAS 9007-07-7) in the presence of DNAse (Sigma, CAS 9003-98-9), followed by mechanical dissociation and centrifugation through a cushion of 4% bovine serum albumin (Sigma, CAS 9048-46-8). These steps were completed using Hibernate medium (ThermoFisher). Cells were then plated onto Poly-L-Lysine (Sigma, CAS 9001-73-4) coated coverslips in 24 well plates. For each coverslip, 25-30 k cells were allowed to settle in a 40 µL drop for approximately 30 min and then each well was filled with 500 µL of NeurobasalA/B27 growth medium (Invitrogen) supplemented with GlutaMax (0.25%, Invitrogen), glutamine (0.25-0.5 mM, Sigma), penicillin/streptomycin (1:100, ThermoFisher), and heat-inactivated fetal calf serum (10%, Sigma, CAS 1943609-65-1). Media was partially exchanged on day 3 (800 µL) and day 14 (500 µL) with fresh maintenance medium comprised of BrainPhys (StemCell), B27 (2%, Invitrogen), GlutaMax (0.25%, Invitrogen), and penicillin/streptomycin (1%, ThermoFisher). Cultures were maintained for up to 2-3 weeks at 37°C and 5% $CO_2$ until use.

**Electrophysiology**

Postsynaptic patch-clamp recordings were performed at mouse cortical neurons [days *in vitro* (DIV) 15-16] using a HEKA EPC10 amplifier (HEKA Elektronik). Pipette solution for voltage-clamp

recordings contained 120 mM CsCl, 20 mM TEA-Cl, 10 mM HEPES, 5 mM EGTA, 3 mM Mg-ATP, 0.3 mM Na-GTP, 5 mM Na-Phosphocreatin, and 3 mM QX314-Cl. The pH was adjusted with CsOH to 7.31 and osmolarity was adjusted with sucrose to 298 mOsm. Series resistance (Rs) was, on average, 9.5 ± 2.3 MΩ and was compensated to remaining Rs of 5.1 ± 0.8 MΩ. Pipettes were pulled from borosilicate glass (Science Products) with a DMZ Universal Electrode (Zeitz Instruments) with a resistance of 3-4 MΩ. Recordings were performed at room temperature.

Recordings of the holding current ($I_{hold}$) and spontaneous inhibitory postsynaptic currents (sIPSCs) were performed at a holding potential of -60 mV in extracellular Tyrode's salt solution containing 145 mM NaCl, 2.5 mM KCl, 1.2 mM $MgCl_2$, 2 mM $CaCl_2$, 10 mM HEPES, and 10 mM glucose. The pH was adjusted by NaOH to 7.4. To isolate $GABA_A$R-mediated currents, the extracellular solution was supplemented by 10 µM NBQX (Biotechne, CAS 479347-86-9) to block AMPA receptors and 50 µM APV (Tocris, CAS 79055-68-8) to block NMDA receptors. Voltages were not corrected for a calculated liquid junction potential of 2 mV. After establishing a baseline recording period (before condition ~3 min), 10 µM chlorophene was washed in through the perfusion system and $I_{hold}$ was monitored. After four min, 50 µM picrotoxin (Sigma, CAS 124-87-8) and 20 µM SR95531 (Sigma, CAS 104104-50-9) were bath-applied to block $GABA_A$R-mediated chloride conductance. To compare $I_{hold}$ before and during the application of chlorophene and after application of the $GABA_A$R blockers, the mean $I_{hold}$ was calculated for (i) the before period ($I_{hold}$ ctr), (ii) 2 min after application of chlorophene ($I_{hold}$ +chloro), and (iii) 1 min after application of picrotoxin and SR95531 ($I_{hold}$ +PTX/SR) for each cell. The main effect of drug perfusion was tested with repeated measures ANOVA followed by pairwise comparisons (Bonferroni t-test, n=6 neurons).

To evaluate the effect of chlorophene on NMDA-evoked currents, NMDA currents were pharmacologically isolated by supplementing the extracelluar solution with 50 µM picrotoxin to block $GABA_A$ receptors and 10 µM NBQX to block AMPA receptors. After establishing a stable baseline recording period, NMDA (1 µM, 10 µM or 20 µM, Merck, CAS 6384-92-5) was washed in through the perfusion system and the change of $I_{hold}$, representing a NMDA evoked current, was monitored. After reaching a stable NMDA evoked current (~3 min) chlorophene was bath applied. In a subset of cells, 50 µM APV was applied at the end of the experiment to block NMDA evoked currents. To compare the effect of chlorophene and APV exposure on NMDA currents, $I_{hold}$ was calculated (i) 3 min after NMDA application ($I_{hold}$ +NMDA), (ii) 2 min after chlorophene application ($I_{hold}$ +chloro) and (iii) 1 min after APV application ($I_{hold}$ +APV). The effect of chlorophene on NMDA currents was compared by a paired t-test ($I_{hold}$ +NMDA vs. $I_{hold}$ +chloro) and for the subset of cells

with APV application by repeated measures ANOVA followed by pairwise comparisons (Bonferroni t-test).

The pipette solution for current clamp recordings contained 115 mM $KMeSO_3$, 5 mM NaCl, 10 mM HEPES, 0.1 mM EGTA, 4 mM Mg-ATP, 0.3 mM Na-GTP, 20 mM $K_2$-Phosphocreatin. The pH was adjusted with KOH to 7.33 and osmolarity was adjusted with sucrose to 298 mOsm. Voltages were not corrected for a calculated liquid junction potential of 9.6 mV. To test the effect of chlorophene on basal neuronal properties and neuronal firing the internal chloride concentration was set to 5 mM to mimic physiological chloride gradients and hyperpolarizing $GABA_A$ receptor-mediated conductance. To isolate the effect of chlorophene via $GABA_A$ receptors, the extracelluar solution was supplemented by 10 µM NBQX and 50 µM APV to block AMPA and NMDA receptors. The built-in bridge compensation was adjusted to 100% of the series resistance determined in voltage-clamp. Passive and active neuronal properties of single neurons were measured before (control) and after chlorophene application, respectively. The input resistance ($R_{in}$) was calculated from alternating subthreshold current injections from −50 to 20 pA (10 pA steps, 200 ms duration). Action potential firing was evoked by suprathreshold depolarizing current injections. The current threshold required for eliciting an action potential was denoted as rheobase. The action potential frequency was calculated from the number of action potentials in response to a 200 ms current injection with an amplitude twice as large as the rheobase. The resting membrane potential ($V_{rest}$) was measured ~1 min after obtaining whole-cell access as the membrane voltage with zero current in current clamp mode. For statistical comparison of neuronal properties under control and chlorophene condition, p values were calculated by paired t-tests.

**Human multi-neurotransmitter receptor (hMNR) assay**

The human multi-neurotransmitter (hMNR) assay used 3D BrainSpheres derived from human-induced pluripotent stem cell (hiPSC)-based neural progenitor cells (hiNPCs). The cultivation of the hiPSC line IMR90 (clone 4, WiCell, Madison, WI, USA), including neural induction, was carried out according to a previously described 2D-NIM protocol[146]. Briefly, hiPSC colonies were singularized and cultured in defined medium, including dual SMAD inhibitors SB-431542 and LDN-193189 for 21 d in 2D. On day 21 of neural induction, hiNPCs were cryopreserved in single-cell suspension. For sphere generation, hiNPCs were thawed, transferred to 6-well plates, and cultivated in a gyrical shaking incubator (140 rpm, 12.5 mm diameter) in a proliferation medium[146]. To start the 3D neural differentiation, hiNPC spheres (0.3 mm in diameter) were cultivated in CINDA+ differentiation medium[146,147] for 3 weeks, and half of the medium was replaced twice weekly. After 3D differentiation, BrainSpheres were plated on pre-coated (Poly-L-Ornithine, Laminin LN521) 96-well microelectrode arrays (MEA, #M768-tMEA-96B, Axion Biosystems) in

CINDA+ differentiation medium (1 sphere per well) and fed twice per week by replacing half of the medium. After 4 weeks of differentiation on the MEAs, spontaneous electrical baseline activity was recorded with the Axion Maestro Pro MEA system. For initial unit identification, BrainSpheres were acutely exposed to the respective neurotransmitter agonists including glutamate (50 µM), and γ-aminobutyric acid (GABA; 10 µM). After electrical activity was measured, neurotransmitter antagonists were added to each well (10 µM bicuculline, 50 µM/50 µM D-AP5/NBQX), network activity was recorded and substances were removed with a complete exchange of the medium. After a 3 h washout, the second baseline was recorded and chlorophene was gradually added at sequentially increasing concentrations (0.25, 0.74, 2.22, 6.67, 20 µM). Extracellular recording of electrical activity was performed for 15 min at 37°C and 5% $CO_2$ in the Axion Maestro Pro System (Axion Biosystems), in line with previous work[146]. For further analysis of detected spikes, recorded .spk files were concatenated in the order of measurement and converted into a single .nex file with a MATLAB (R2021b, R2022b, MathWorks, Natick, MA, USA) script. Spike sorting of the .nex file was performed using the Offline Sorter (OFS, version 4.4, Plexon, Dallas, TX, USA) software, applying the automatic clustering T-Distribution EM method with 10 degrees of freedom (DOF) and an initial number of units of 20. The sorted units were exported as per-unit and per-waveform data. BrainSphere spiking data was analyzed using a custom KNIME (version 4.1.4, KNIME AG, www.knime.com) workflow implemented with R scripts[133] for statistical analysis and data visualization using the add-on package ggplot2[134]. For determination of neuronal subtype-specific responses, only units responding with a minimum fold change of 0.25 (increase or decrease) to the respective neurotransmitter and neurotransmitter receptor antagonist treatment compared to the baseline recording were analyzed for a specific response to chlorophene. Units were classified as GABAergic if, relative to the first baseline recording, the fold change in spiking following bicuculline (10 µM) and GABA (10 µM) treatments were ≤0.75 and ≥1.25, respectively Similarly, units were defined as glutamatergic if glutamate (50 µM) increased baseline spiking activity by factor ≥1.25, and if APV/NBQX (50 µM/50 µM) reduced spiking relative to prior glutamate treatment by factor ≤0.75. To account for differences in baseline spiking frequency between individual electrodes, the weighted mean firing rate (wMFR), representing the number of recorded spikes per second and recording, was scaled to the sum of wMFRs across all recordings including both the second baseline recording and subsequent recordings under chlorophene exposure. To ease visual data accessibility, scaled wMFRs were shifted by 1-$\text{median}_{\text{control}}$ to set the control median to one. As described above, a two-sample bootstrapping test and Benjamini-Hochberg correction were used to calculate p-values and to determine significant differences between control and treatment groups.

752

## References


1. Persson, L. *et al.* Outside the Safe Operating Space of the Planetary Boundary for Novel Entities. *Environ. Sci. Technol.* **56**, 1510–1521 (2022).

2. Wang, Z., Walker, G. W., Muir, D. C. G. & Nagatani-Yoshida, K. Toward a Global Understanding of Chemical Pollution: A First Comprehensive Analysis of National and Regional Chemical Inventories. *Environ. Sci. Technol.* **54**, 2575–2584 (2020).

3. Landrigan, P. J. *et al.* The Lancet Commission on pollution and health. *The Lancet* **391**, 462–512 (2018).

4. Fuller, R. *et al.* Pollution and health: a progress update. *The Lancet Planetary Health* **6**, e535–e547 (2022).

5. Harris, J. B. Neurotoxicology: what the neurologist needs to know. *Journal of Neurology, Neurosurgery & Psychiatry* **75**, iii29–iii34 (2004).

6. Spivey, A. Rotenone and Paraquat Linked to Parkinson's Disease: Human Exposure Study Supports Years of Animal Studies. *Environ Health Perspect* **119**, a (2011).

7. Weisskopf, M. G. *et al.* Association of Cumulative Lead Exposure with Parkinson's Disease. *Environ Health Perspect* **118**, 1609–1613 (2010).

8. Elonheimo, H. M., Andersen, H. R., Katsonouri, A. & Tolonen, H. Environmental Substances Associated with Alzheimer's Disease—A Scoping Review. *IJERPH* **18**, 11839 (2021).

9. Billioti De Gage, S. *et al.* Benzodiazepine use and risk of Alzheimer's disease: case-control study. *BMJ* **349**, g5205–g5205 (2014).

10. Lu, C. & Tune, L. E. Chronic Exposure to Anticholinergic Medications Adversely Affects the Course of Alzheimer Disease. *The American Journal of Geriatric Psychiatry* **11**, 458–461 (2003).

11. Yousef, S. *et al.* Attention Deficit Hyperactivity Disorder and Environmental Toxic Metal Exposure in the United Arab Emirates. *Journal of Tropical Pediatrics* **57**, 457–460 (2011).

12. Moore, S. *et al.* The Association between ADHD and Environmental Chemicals—A Scoping Review. *IJERPH* **19**, 2849 (2022).

13. Grandjean, P. & Landrigan, P. J. Neurobehavioural effects of developmental toxicity. *The Lancet Neurology* **13**, 330–338 (2014).

14. McCormack, A. L. *et al.* Environmental Risk Factors and Parkinson's Disease: Selective Degeneration of Nigral Dopaminergic Neurons Caused by the Herbicide Paraquat. *Neurobiology of Disease* **10**, 119–127 (2002).

15. Moreno, J. A. *et al.* Age-Dependent Susceptibility to Manganese-Induced Neurological Dysfunction. *Toxicological Sciences* **112**, 394–404 (2009).

16. Eriksson, P., Jakobsson, E. & Fredriksson, A. Brominated flame retardants: a novel class of developmental neurotoxicants in our environment? *Environ Health Perspect* **109**, 903–908 (2001).

788 17. Branchi, I., Alleva, E. & Costa, L. G. Effects of Perinatal Exposure to a Polybrominated Diphenyl
789 Ether (PBDE 99) on Mouse Neurobehavioural Development. *NeuroToxicology* **23**, 375–384 (2002).

790 18. Eriksson, P., Viberg, H., Jakobsson, E., Orn, U. & Fredriksson, A. A Brominated Flame Retardant,
791 2,2`,4,4`,5-Pentabromodiphenyl Ether: Uptake, Retention, and Induction of Neurobehavioral Alterations
792 in Mice during a Critical Phase of Neonatal Brain Development. *Toxicological Sciences* **67**, 98–103 (2002).

793 19. Zhou, C.-C. *et al.* Lead exposure induces Alzheimers's disease (AD)-like pathology and disturbes
794 cholesterol metabolism in the young rat brain. *Toxicology Letters* **296**, 173–183 (2018).

795 20. Ossowska, K. *et al.* A slowly developing dysfunction of dopaminergic nigrostriatal neurons
796 induced by long-term paraquat administration in rats: an animal model of preclinical stages of
797 Parkinson's disease? *Eur J of Neuroscience* **22**, 1294–1304 (2005).

798 21. Wu, J. *et al.* Alzheimer's Disease (AD)-Like Pathology in Aged Monkeys after Infantile Exposure to
799 Environmental Metal Lead (Pb): Evidence for a Developmental Origin and Environmental Link for AD. *J.*
800 *Neurosci.* **28**, 3–9 (2008).

801 22. Masilamoni, G. J. & Smith, Y. Chronic MPTP administration regimen in monkeys: a model of
802 dopaminergic and non-dopaminergic cell loss in Parkinson's disease. *J Neural Transm* **125**, 337–363
803 (2018).

804 23. Lee, J. & Freeman, J. L. Zebrafish as a model for investigating developmental lead (Pb)
805 neurotoxicity as a risk factor in adult neurodegenerative disease: A mini-review. *NeuroToxicology* **43**, 57–
806 64 (2014).

807 24. Yen, P.-L., How, C. M. & Hsiu-Chuan Liao, V. Early-life and chronic exposure to di(2-ethylhexyl)
808 phthalate enhances amyloid-β toxicity associated with an autophagy-related gene in Caenorhabditis
809 elegans Alzheimer's disease models. *Chemosphere* **273**, 128594 (2021).

810 25. Martin, M. M. *et al.* An expert-driven literature review of "negative" chemicals for
811 developmental neurotoxicity (DNT) in vitro assay evaluation. *Neurotoxicology and Teratology* **93**, 107117
812 (2022).

813 26. OECD. *Test No. 424: Neurotoxicity Study in Rodents*. (OECD, 1997). doi:10.1787/9789264071025-
814 en.

815 27. OECD. *Test No. 426: Developmental Neurotoxicity Study*. (OECD, 2007).
816 doi:10.1787/9789264067394-en.

817 28. U.S. Environmental Protection Agency. Health Effects Guidelines OPPTS 870.6300 Developmental
818 Neurotoxicity Study. https://nepis.epa.gov/Exe/ZyPURL.cgi?Dockey=P100IRWO.txt (1998).

819 29. Crofton, K. M., Mundy, W. R. & Shafer, T. J. Developmental neurotoxicity testing: A path forward.
820 *Congenital Anomalies* **52**, 140–146 (2012).

821 30. Tohyama, C. Developmental neurotoxicity test guidelines: problems and perspectives. *J. Toxicol.*
822 *Sci.* **41**, SP69–SP79 (2016).

823 31. Smirnova, L. Developmental neurotoxicity – Challenges in the 21st Century and In Vitro
824 Opportunities. *ALTEX* (2014) doi:10.14573/altex.1403271.

825 32. *Toxicity Testing in the 21st Century: A Vision and a Strategy*. (The National Academies Press,
826 Washington, DC, 2007).

827 33. Tal, T. *et al.* New approach methods to assess developmental and adult neurotoxicity for
828 regulatory use: a PARC work package 5 project. *Front. Toxicol.* **6**, 1359507 (2024).

829 34. Crofton, K. M. *et al.* Current status and future directions for a neurotoxicity hazard assessment
830 framework that integrates in silico approaches. *Computational Toxicology* **22**, 100223 (2022).

831 35. Sachana, M. *et al.* International Regulatory and Scientific Effort for Improved Developmental
832 Neurotoxicity Testing. *Toxicological Sciences* **167**, 45–57 (2019).

833 36. Blum, J. *et al.* Establishment of a human cell-based in vitro battery to assess developmental
834 neurotoxicity hazard of chemicals. *Chemosphere* **311**, 137035 (2023).

835 37. Howe, K. *et al.* The zebrafish reference genome sequence and its relationship to the human
836 genome. *Nature* **496**, 498–503 (2013).

837 38. Strähle, U. *et al.* Zebrafish embryos as an alternative to animal experiments—A commentary on
838 the definition of the onset of protected life stages in animal welfare regulations. *Reproductive Toxicology*
839 **33**, 128–132 (2012).

840 39. European Parliament, Council of the European Union. Directive 2010/63/EU of the European
841 Parliament and of the Council of 22 September 2010 on the protection of animals used for scientific
842 purposes Text with EEA relevance. (2010).

843 40. Cassar, S. *et al.* Use of Zebrafish in Drug Discovery Toxicology. *Chem. Res. Toxicol.* **33**, 95–118
844 (2020).

845 41. Kimmel, C. B., Ballard, W. W., Kimmel, S. R., Ullmann, B. & Schilling, T. F. Stages of embryonic
846 development of the zebrafish. *Developmental Dynamics* **203**, 253–310 (1995).

847 42. Brustein, E., Marandi, N., Kovalchuk, Y., Drapeau, P. & Konnerth, A. 'In vivo' monitoring of
848 neuronal network activity in zebrafish by two-photon Ca2+ imaging. *Pflugers Arch - Eur J Physiol* **446**,
849 766–773 (2003).

850 43. Fetcho, J. R. & O'Malley, D. M. Visualization of active neural circuitry in the spinal cord of intact
851 zebrafish. *Journal of Neurophysiology* **73**, 399–406 (1995).

852 44. Burgess, H. A. & Granato, M. Sensorimotor Gating in Larval Zebrafish. *J. Neurosci.* **27**, 4984–4994
853 (2007).

854 45. Burgess, H. A. & Granato, M. Modulation of locomotor activity in larval zebrafish during light
855 adaptation. *Journal of Experimental Biology* **210**, 2526–2539 (2007).

856 46. Wolman, M. A., Jain, R. A., Liss, L. & Granato, M. Chemical modulation of memory formation in
857 larval zebrafish. *Proc. Natl. Acad. Sci. U.S.A.* **108**, 15468–15473 (2011).

858 47. Best, J. D. *et al.* Non-Associative Learning in Larval Zebrafish. *Neuropsychopharmacol* **33**, 1206–
859 1215 (2008).

860 48. Bruni, G. *et al.* Zebrafish behavioral profiling identifies multitarget antipsychotic-like compounds.
861 *Nat Chem Biol* **12**, 559–566 (2016).

862 49. Jordi, J. *et al.* High-throughput screening for selective appetite modulators: A multibehavioral
863 and translational drug discovery strategy. *Sci. Adv.* **4**, eaav1966 (2018).

864 50. Kokel, D. *et al.* Rapid behavior-based identification of neuroactive small molecules in the
865 zebrafish. *Nat Chem Biol* **6**, 231–237 (2010).

866 51. McCarroll, M. N. *et al.* Zebrafish behavioural profiling identifies GABA and serotonin receptor
867 ligands related to sedation and paradoxical excitation. *Nat Commun* **10**, 4078 (2019).

868 52. Babin, P. J., Goizet, C. & Raldúa, D. Zebrafish models of human motor neuron diseases:
869 Advantages and limitations. *Progress in Neurobiology* **118**, 36–58 (2014).

870 53. Bandmann, O. & Burton, E. A. Genetic zebrafish models of neurodegenerative diseases.
871 *Neurobiology of Disease* **40**, 58–65 (2010).

872 54. Lee, J. & Freeman, J. Zebrafish as a Model for Developmental Neurotoxicity Assessment: The
873 Application of the Zebrafish in Defining the Effects of Arsenic, Methylmercury, or Lead on Early
874 Neurodevelopment. *Toxics* **2**, 464–495 (2014).

875 55. Rankin, C. H. *et al.* Habituation revisited: An updated and revised description of the behavioral
876 characteristics of habituation. *Neurobiology of Learning and Memory* **92**, 135–138 (2009).

877 56. Riedel, G. Glutamate receptor function in learning and memory. *Behavioural Brain Research* **140**,
878 1–47 (2003).

879 57. Li, F. & Tsien, J. Z. Memory and the NMDA Receptors. *N Engl J Med* **361**, 302–303 (2009).

880 58. Hunt, D. L. & Castillo, P. E. Synaptic plasticity of NMDA receptors: mechanisms and functional
881 implications. *Current Opinion in Neurobiology* **22**, 496–508 (2012).

882 59. Williams, A. J. *et al.* The CompTox Chemistry Dashboard: a community data resource for
883 environmental chemistry. *J Cheminform* **9**, 61 (2017).

884 60. Kumar Singh, A., Nath Tiwari, M., Prakash, O. & Pratap Singh, M. A Current Review of
885 Cypermethrin-Induced Neurotoxicity and Nigrostriatal Dopaminergic Neurodegeneration. *CN* **10**, 64–71
886 (2012).

887 61. EFSA Panel on Plant Protection Products and their Residues (EFSA PPR Panel) *et al.* Development
888 of Integrated Approaches to Testing and Assessment (IATA) case studies on developmental neurotoxicity
889 (DNT) risk assessment. *EFS2* **19**, (2021).

890 62. European Chemicals Agency. Product-type 3 Assessment report: Chlorophene. (2017).

891 63. Safety Assessment of Dichlorophene and Chlorophene1. *Int J Toxicol* **23**, 1–27 (2004).

892 64. Keiser, M. J. *et al.* Relating protein pharmacology by ligand chemistry. *Nat Biotechnol* **25**, 197–
893 206 (2007).

894 65. Emran, F., Rihel, J. & Dowling, J. E. A Behavioral Assay to Measure Responsiveness of Zebrafish to
895 Changes in Light Intensities. *JoVE* 923 (2008) doi:10.3791/923.

896 66. Jarema, K. A. *et al.* Developmental Neurotoxicity and Behavioral Screening in Larval Zebrafish
897 with a Comparison to Other Published Results. *Toxics* **10**, 256 (2022).

898 67. Gaballah, S. *et al.* Evaluation of Developmental Toxicity, Developmental Neurotoxicity, and
899 Tissue Dose in Zebrafish Exposed to GenX and Other PFAS. *Environ Health Perspect* **128**, 047005 (2020).

900 68. Leuthold, D., Klüver, N., Altenburger, R. & Busch, W. Can Environmentally Relevant Neuroactive
901 Chemicals Specifically Be Detected with the Locomotor Response Test in Zebrafish Embryos? *Environ. Sci.*
902 *Technol.* **53**, 482–493 (2019).

903 69. Kavšek, M. Predicting later IQ from infant visual habituation and dishabituation: A meta-analysis.
904 *Journal of Applied Developmental Psychology* **25**, 369–393 (2004).

905 70. McCall, R. B. & Carriger, M. S. A Meta-Analysis of Infant Habituation and Recognition Memory
906 Performance as Predictors of Later IQ. *Child Development* **64**, 57 (1993).

907 71. McDiarmid, T. A., Bernardos, A. C. & Rankin, C. H. Habituation is altered in neuropsychiatric
908 disorders—A comprehensive review with recommendations for experimental design and analysis.
909 *Neuroscience & Biobehavioral Reviews* **80**, 286–305 (2017).

910 72. Valsamis, B. & Schmid, S. Habituation and Prepulse Inhibition of Acoustic Startle in Rodents. *JoVE*
911 3446 (2011) doi:10.3791/3446.

912 73. Ludewig, K. *et al.* The acoustic startle reflex and its modulation: effects of age and gender in
913 humans. *Biological Psychology* **63**, 311–323 (2003).

914 74. Roberts, A. C. *et al.* Long-term habituation of the C-start escape response in zebrafish larvae.
915 *Neurobiology of Learning and Memory* **134**, 360–368 (2016).

916 75. Roberts, A. C. *et al.* Habituation of the C-Start Response in Larval Zebrafish Exhibits Several
917 Distinct Phases and Sensitivity to NMDA Receptor Blockade. *PLoS ONE* **6**, e29132 (2011).

918 76. Morris, R. Synaptic plasticity and learning: selective impairment of learning rats and blockade of
919 long-term potentiation in vivo by the N-methyl-D- aspartate receptor antagonist AP5. *J. Neurosci.* **9**,
920 3040–3057 (1989).

921 77. Wozniak, D. F., Olney, J. W., Kettinger, L., Price, M. & Miller, J. P. Behavioral effects of MK-801 in
922 the rat. *Psychopharmacology* **101**, 47–56 (1990).

923 78. Paoletti, P., Bellone, C. & Zhou, Q. NMDA receptor subunit diversity: impact on receptor
924 properties, synaptic plasticity and disease. *Nat Rev Neurosci* **14**, 383–400 (2013).

925 79. Zoodsma, J. D. *et al.* A Model to Study NMDA Receptors in Early Nervous System Development. *J.*
926 *Neurosci.* **40**, 3631–3645 (2020).

927 80. Galligan, J. J. & North, R. A. MK-801 blocks nicotinic depolarizations of guinea pig myenteric
928 neurons. *Neuroscience Letters* **108**, 105–109 (1990).

929 81. Rothman, S. Noncompetitive N-methyl-D-aspartate antagonists affect multiple ionic currents. *J*
930 *Pharmacol Exp Ther* **246**, 137–142 (1988).

931 82. Mancuso, C. E., Tanzi, M. G. & Gabay, M. Paradoxical Reactions to Benzodiazepines: Literature
932 Review and Treatment Options. *Pharmacotherapy* **24**, 1177–1185 (2004).

933 83. McCarthy, M. M., Brown, E. N. & Kopell, N. Potential Network Mechanisms Mediating
934 Electroencephalographic Beta Rhythm Changes during Propofol-Induced Paradoxical Excitation. *J.*
935 *Neurosci.* **28**, 13488–13504 (2008).

936 84. Reddy, R. V., Moorthy, S. S., Dierdorf, S. F., Deitch, R. D. & Link, L. Excitatory Effects and
937 Electroencephalographic Correlation of Etomidate, Thiopental, Methohexital, and Propofol: *Anesthesia &*
938 *Analgesia* **77**, 1008???1011 (1993).

939 85. Iqbal, F. *et al.* Anesthetics: from modes of action to unconsciousness and neurotoxicity. *Journal*
940 *of Neurophysiology* **122**, 760–787 (2019).

941 86. Århem, P., Klement, G. & Nilsson, J. Mechanisms of Anesthesia: Towards Integrating Network,
942 Cellular, and Molecular Level Modeling. *Neuropsychopharmacol* **28**, S40–S47 (2003).

943 87. Armstrong, R. *et al.* Mechanisms of Anesthetic Action and Neurotoxicity: Lessons from Molluscs.
944 *Front. Physiol.* **8**, 1138 (2018).

945 88. Franks, N. P. & Lieb, W. R. Molecular and cellular mechanisms of general anaesthesia. *Nature*
946 **367**, 607–614 (1994).

947 89. Sun, L. Early childhood general anaesthesia exposure and neurocognitive development. *British*
948 *Journal of Anaesthesia* **105**, i61–i68 (2010).

949 90. Monesson-Olson, B. *et al.* Expression of the eight GABAA receptor α subunits in the developing
950 zebrafish central nervous system. *PLoS ONE* **13**, e0196083 (2018).

951 91. Sadamitsu, K. *et al.* Characterization of zebrafish GABAA receptor subunits. *Sci Rep* **11**, 6242
952 (2021).

953 92. Collinson, N. *et al.* Enhanced Learning and Memory and Altered GABAergic Synaptic Transmission
954 in Mice Lacking the α5 Subunit of the $GABA_A$ Receptor. *J. Neurosci.* **22**, 5572–5580 (2002).

955 93. Crestani, F. *et al.* Trace fear conditioning involves hippocampal $\alpha_5$ $GABA_A$ receptors. *Proc. Natl.*
956 *Acad. Sci. U.S.A.* **99**, 8980–8985 (2002).

957 94. Yee, B. K. *et al.* $GABA_A$ receptors containing the α5 subunit mediate the trace effect in aversive
958 and appetitive conditioning and extinction of conditioned fear. *Eur J of Neuroscience* **20**, 1928–1936
959 (2004).

960 95. Navarro, J. F., Burón, E. & Martín-López, M. Anxiogenic-like activity of L-655,708, a selective
961 ligand for the benzodiazepine site of GABAA receptors which contain the alpha-5 subunit, in the elevated
962 plus-maze test. *Progress in Neuro-Psychopharmacology and Biological Psychiatry* **26**, 1389–1392 (2002).

963 96. Atack, J. R. *et al.* L-655,708 enhances cognition in rats but is not proconvulsant at a dose
964 selective for α5-containing GABAA receptors. *Neuropharmacology* **51**, 1023–1029 (2006).

965 97. Dawson, G. R. *et al.* An Inverse Agonist Selective for α5 Subunit-Containing $GABA_A$ Receptors
966 Enhances Cognition. *J Pharmacol Exp Ther* **316**, 1335–1345 (2006).

967 98. Ballard, T. M. *et al.* RO4938581, a novel cognitive enhancer acting at GABAA α5 subunit-
968 containing receptors. *Psychopharmacology* **202**, 207–223 (2009).

969 99. Herbison, A. E. & Moenter, S. M. Depolarising and Hyperpolarising Actions of GABAA Receptor
970 Activation on Gonadotrophin-Releasing Hormone Neurones: Towards an Emerging Consensus: GABAA
971 modulation of GnRH neurones. *Journal of Neuroendocrinology* **23**, 557–569 (2011).

972 100. Cui, Y. *et al.* Neurofibromin Regulation of ERK Signaling Modulates GABA Release and Learning.
973 *Cell* **135**, 549–560 (2008).

974 101. Yoshiike, Y. *et al.* GABAA Receptor-Mediated Acceleration of Aging-Associated Memory Decline
975 in APP/PS1 Mice and Its Pharmacological Treatment by Picrotoxin. *PLoS ONE* **3**, e3029 (2008).

976 102. Portavella, M., Vargas, J. P., Torres, B. & Salas, C. The effects of telencephalic pallial lesions on
977 spatial, temporal, and emotional learning in goldfish. *Brain Research Bulletin* **57**, 397–399 (2002).

978 103. Rodríguez, F. *et al.* Spatial memory and hippocampal pallium through vertebrate evolution:
979 insights from reptiles and teleost fish. *Brain Research Bulletin* **57**, 499–503 (2002).

980 104. Saleem, S. & Kannan, R. R. Zebrafish: an emerging real-time model system to study Alzheimer's
981 disease and neurospecific drug discovery. *Cell Death Discov.* **4**, 45 (2018).

982 105. Nam, R.-H., Kim, W. & Lee, C.-J. NMDA receptor-dependent long-term potentiation in the
983 telencephalon of the zebrafish. *Neuroscience Letters* **370**, 248–251 (2004).

984 106. Tsien, J. Z. Building a Brainier Mouse. *Sci Am* **282**, 62–68 (2000).

985 107. Newcomer, J. W. & Krystal, J. H. NMDA receptor regulation of memory and behavior in humans.
986 *Hippocampus* **11**, 529–542 (2001).

987 108. Brown, D. A. & Passmore, G. M. Neural *KCNQ* (Kv7) channels. *British J Pharmacology* **156**, 1185–
988 1195 (2009).

989 109. De Leon, J. & Nikoloff, D. M. Paradoxical Excitation on Diphenhydramine May Be Associated with
990 Being a CYP2D6 Ultrarapid Metabolizer: *Three Case Reports*. *CNS spectr.* **13**, 133–135 (2008).

991 110. National Industrial Chemicals Notification and Assessment Scheme. Chlorophene preservatives:
992 Environment tier II assessment. (2019).

993 111. Yu, J. T., Bouwer, E. J. & Coelhan, M. Occurrence and biodegradability studies of selected
994 pharmaceuticals and personal care products in sewage effluent. *Agricultural Water Management* **86**, 72–
995 80 (2006).

996 112. Kasprzyk-Hordern, B., Dinsdale, R. M. & Guwy, A. J. The removal of pharmaceuticals, personal
997 care products, endocrine disruptors and illicit drugs during wastewater treatment and its impact on the
998 quality of receiving waters. *Water Research* **43**, 363–380 (2009).

999 113. REACH. REACH Dossier for Chlorofene. (2019).

1000 114. OECD. *Test No. 210: Fish, Early-Life Stage Toxicity Test*. (OECD, 2013).
1001 doi:10.1787/9789264203785-en.

1002 115. Kleinstreuer, N. C. *et al.* Development and Validation of a Computational Model for Androgen
1003 Receptor Activity. *Chem. Res. Toxicol.* **30**, 946–964 (2017).

1004 116. The European Parliament and the Council of the European Union. Regulation (EC) No 1272/2008
1005 of the European Parliament and of the Council of 16 December 2008 on classification, labelling and
1006 packaging of substances and mixtures, amending and repealing Directives 67/548/EEC and 1999/45/EC,
1007 and amending Regulation (EC) No 1907/2006. (2008).

1008 117. European Chemicals Agency. Minutes of the 62nd Meeting of the Committee for Risk
1009 Assessment (RAC-62). (2022).

1010 118. European Chemicals Agency. *Guidance on Information Requirements and Chemical Safety*
1011 *Assessment: Chapter R.7a : Endpoint Specific Guidance.* (Publications Office, LU, 2017).

1012 119. European Chemicals Agency. *Non-Animal Approaches: Current Status of Regulatory Applicability*
1013 *under the REACH, CLP and Biocidal Products Regulations.* (Publications Office, LU, 2017).

1014 120. European Chemicals Agency. *Guidance on the Biocidal Products Regulation: Volume III : Human*
1015 *Health, Assessment and Evaluation (Parts B+C).* (Publications Office, LU, 2017).

1016 121. Kenda, M., Karas Kuželički, N., Iida, M., Kojima, H. & Sollner Dolenc, M. Triclocarban, Triclosan,
1017 Bromochlorophene, Chlorophene, and Climbazole Effects on Nuclear Receptors: An *in Silico* and *in Vitro*
1018 Study. *Environ Health Perspect* **128**, 107005 (2020).

1019 122. Gladkevich, A., Korf, J., Hakobyan, V. P. & Melkonyan, K. V. The peripheral GABAergic system as a
1020 target in endocrine disorders. *Autonomic Neuroscience* **124**, 1–8 (2006).

1021 123. Casoni, F. *et al.* SDF and GABA interact to regulate axophilic migration of GnRH neurons. *Journal*
1022 *of Cell Science* jcs.101675 (2012) doi:10.1242/jcs.101675.

1023 124. Eepho, O.-I. *et al.* Modulation of GABA by sodium butyrate ameliorates hypothalamic
1024 inflammation in experimental model of PCOS. *BMC Neurosci* **24**, 62 (2023).

1025 125. Ingram, R. J., Leverton, L. K., Daniels, V. C., Li, J. & Christian-Hinman, C. A. Increased GABA
1026 transmission to GnRH neurons after intrahippocampal kainic acid injection in mice is sex-specific and
1027 associated with estrous cycle disruption. *Neurobiology of Disease* **172**, 105822 (2022).

1028 126. European Commission. Communication from the Commission: The European Green Deal. (2019).

1029 127. Fritsche, E. *et al.* Current Availability of Stem Cell-Based In Vitro Methods for Developmental
1030 Neurotoxicity (DNT) Testing. *Toxicological Sciences* **165**, 21–30 (2018).

1031 128. Bal-Price, A. K., Hogberg, H. T., Buzanska, L. & Coecke, S. Relevance of in vitro neurotoxicity
1032 testing for regulatory requirements: Challenges to be considered. *Neurotoxicology and Teratology* **32**,
1033 36–41 (2010).

1034 129. Bally-Cuif, L. & Vernier, P. Organization and physiology of the zebrafish nervous system. in *Fish*
1035 *Physiology* vol. 29 25–80 (Elsevier, 2010).

1036 130. Kaslin, J. & Ganz, J. Zebrafish Nervous Systems. in *The Zebrafish in Biomedical Research* 181–189
1037 (Elsevier, 2020). doi:10.1016/B978-0-12-812431-4.00018-X.

1038 131. Brox, S., Seiwert, B., Küster, E. & Reemtsma, T. Toxicokinetics of Polar Chemicals in Zebrafish
1039 Embryo ( *Danio rerio* ): Influence of Physicochemical Properties and of Biological Processes. *Environ. Sci.*
1040 *Technol.* **50**, 10264–10272 (2016).

1041 132. Loerracher, A.-K. & Braunbeck, T. Cytochrome P450-dependent biotransformation capacities in
1042 embryonic, juvenile and adult stages of zebrafish (Danio rerio)—a state-of-the-art review. *Arch Toxicol*
1043 **95**, 2299–2334 (2021).

1044 133. R Core Team. R: A language and environment for statistical computing. (2021).

1045 134. Wickham, H. *Ggplot2: Elegant Graphics for Data Analysis*. (Springer, Switzerland, 2016).
1046 doi:10.1007/978-3-319-24277-4.

1047 135. Neuwirth, E. RColorBrewer. (2022).

1048 136. Gu, Z. Complex heatmap visualization. *iMeta* **1**, e43 (2022).

1049 137. Lloyd, D. R., Medina, D. J., Hawk, L. W., Fosco, W. D. & Richards, J. B. Habituation of reinforcer
1050 effectiveness. *Front. Integr. Neurosci.* **7**, (2014).

1051 138. Kulesa, A., Krzywinski, M., Blainey, P. & Altman, N. Sampling distributions and the bootstrap. *Nat*
1052 *Methods* **12**, 477–478 (2015).

1053 139. Harpaz, R. *et al.* Collective behavior emerges from genetically controlled simple behavioral
1054 motifs in zebrafish. *Sci. Adv.* **7**, eabi7460 (2021).

1055 140. Efron, B. Bootstrap Methods: Another Look at the Jackknife. *Ann. Statist.* **7**, (1979).

1056 141. de Mendiburu, F. & Yaseen, M. agricolae: Statistical Procedures for Agricultural Research. (2020).

1057 142. Cameron, L. P. *et al.* A non-hallucinogenic psychedelic analogue with therapeutic potential.
1058 *Nature* **589**, 474–479 (2021).

1059 143. Zhang, X. D. A pair of new statistical parameters for quality control in RNA interference high-
1060 throughput screening assays. *Genomics* **89**, 552–561 (2007).

1061 144. Judson, R. *et al.* Editor's Highlight: Analysis of the Effects of Cell Stress and Cytotoxicity on *In*
1062 *Vitro* Assay Activity Across a Diverse Chemical and Assay Space. *Toxicol. Sci.* **152**, 323–339 (2016).

1063 145. Moutin, E. *et al.* Procedures for Culturing and Genetically Manipulating Murine Hippocampal
1064 Postnatal Neurons. *Front. Synaptic Neurosci.* **12**, 19 (2020).

1065 146. Hartmann, J. *et al.* Molecular and Functional Characterization of Different BrainSphere Models
1066 for Use in Neurotoxicity Testing on Microelectrode Arrays. *Cells* **12**, 1270 (2023).

1067 147. Nimtz, L. *et al.* Characterization and application of electrically active neuronal networks
1068 established from human induced pluripotent stem cell-derived neural progenitor cells for neurotoxicity
1069 evaluation. *Stem Cell Research* **45**, 101761 (2020).

1070

## Acknowledgements

We thank [DBPR] for statistical consultation. This work was supported by a [DBPR] grant to [DBPR] and [DBPR] (Grant Agreement No [DBPR]) to [DBPR] and [DBPR].

## Author contributions

[DBPR] designed and performed the research, analyzed the data, and wrote the manuscript. [DBPR], [DBPR], [DBPR], and [DBPR] performed experiments and analyzed data. [DBPR] designed the study and wrote the manuscript. All authors contributed to data interpretation and commented on the manuscript.

## Corresponding authors

Correspondence should be addressed to [DBPR] and [DBPR].

## Ethics declarations

[DBPR] and [DBPR] are shareholders of the company [DBPR] which provides DNT *in vitro* battery assay service. They declare no potential conflict of interest concerning the data included in this article. All other authors declare no competing interests.

## Availability of data and code

All data (DOI: 10.6084/m9.figshare.26819890) and code (DOI: 10.6084/m9.figshare.26819914) were uploaded to FigShare and will be public upon paper acceptance.

## Extended Data

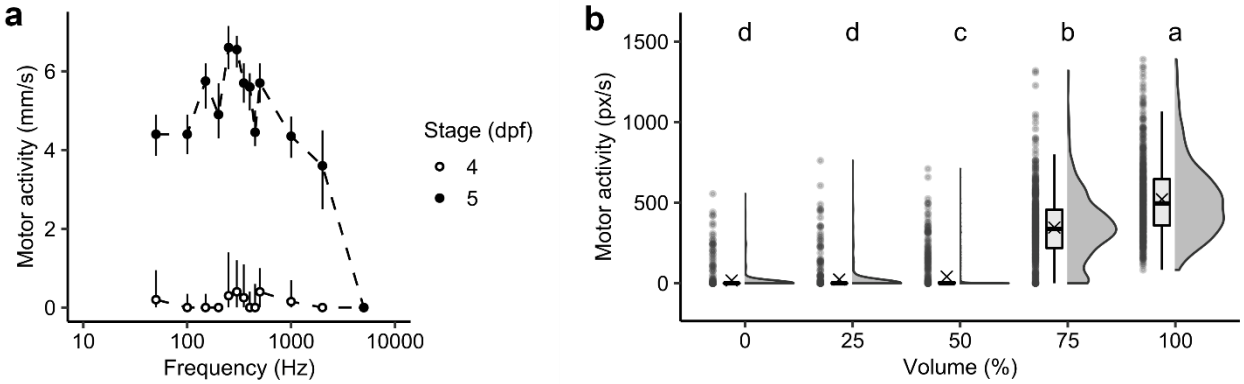


**Extended Data Figure 1 | Developmental stage-, frequency-, and volume-dependency of acoustic startle response and acoustic startle habituation in larval zebrafish.** Parameters considered for establishment of behavior assay battery components based on acoustic stimuli. (**a**) Comparison of responsiveness (y-axis) to 1-second acoustic stimuli (100% volume, 0% light intensity) across different frequencies (x-axis) in 4 and 5 d post-fertilization (dpf) zebrafish larvae. Data shows median ± 95% CI (*n*=192 larvae). (**b**) Acoustic startle response intensity (y-axis) at different nominal volume levels (x-axis) at 5 dpf. Larvae were dark-acclimated for 20 min prior to application of five consecutive acoustic stimuli (1 s, 300 Hz, inter stimulus interval (ISI) 60 s). Acoustic stimulation bouts per volume level were interspaced with inter bout intervals of 5 min. Data points represent average per volume level and individual across five trials. Compact letter display above rainclouds indicates significant differences between volume levels ($p<0.05$, Kruskal-Wallis rank sum test, $n$ = 72 larvae).

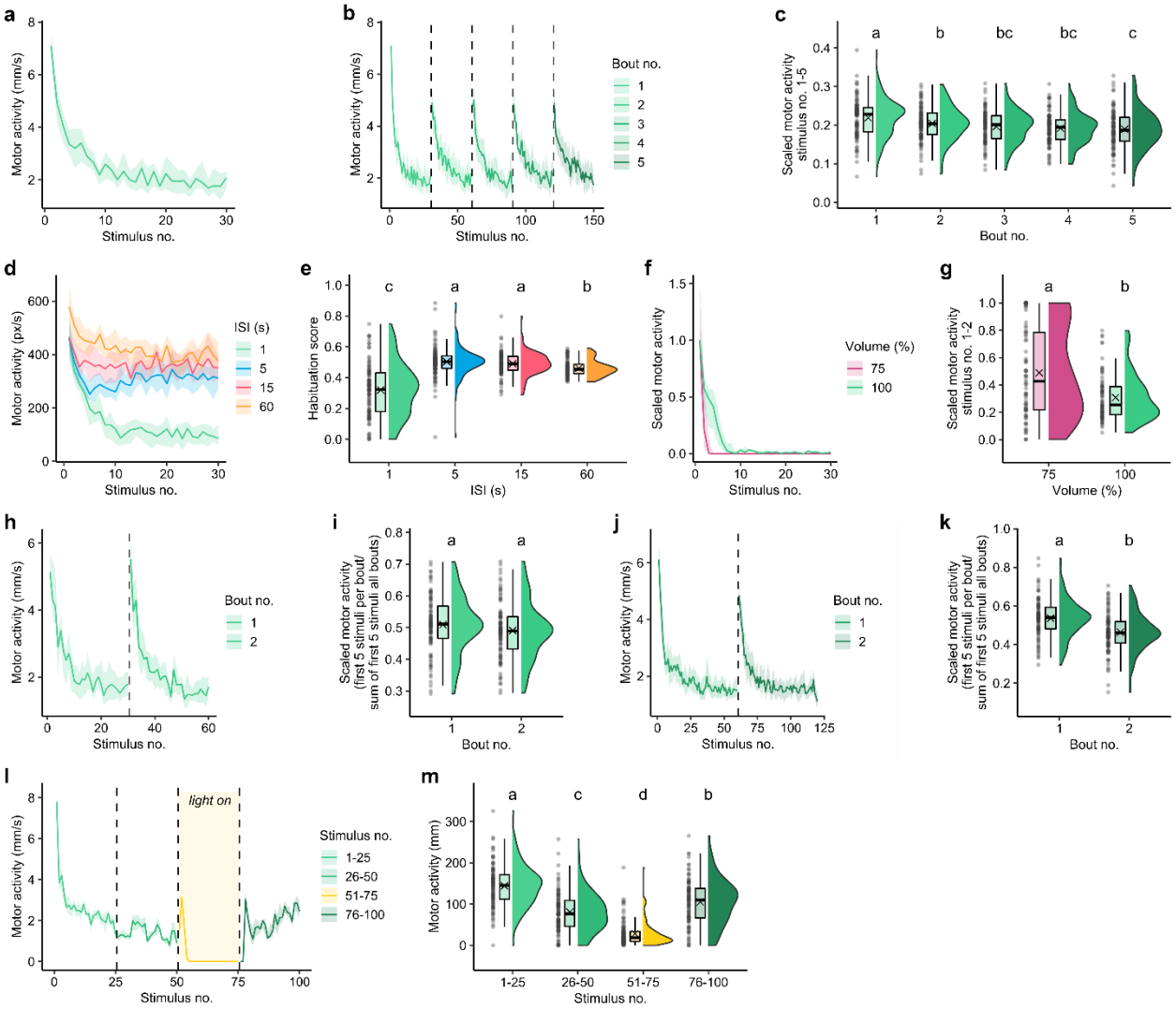


**Extended Data Figure 2 | Characteristics of habituation according to Rankin et al.[55].** (**a**) Progressive response decrease to an asymptotic level. Motor activity (y-axis) of 5-dpf zebrafish larvae over a sequence of 30 consecutive 1-second acoustic stimuli (300 Hz, 100% volume, inter stimulus interval (ISI) 1 s). Data is median ± 95% CI (*n* = 96). (**b, c**) Spontaneous recovery of response after response decrement. Stimulus repetitions and spontaneous recoveries result in more rapid/pronounced habituation (potentiation of habituation). Line graph shows the motor activity (y-axis) of 5-dpf zebrafish larvae over a sequence of five habituation bouts, each consisting of 30 consecutive 1-second acoustic stimuli (x-axis) (300 Hz, 100% volume, ISI = 1 s). Dashed vertical lines indicate inter bout intervals (IBIs) of 1 min. Data is median ± 95% CI (*n* = 96). Raincloud graph shows the cumulative motor activity during the first five stimuli per habituation bout scaled to the overall cumulative motor activity per individual across the first five stimuli (y-axis) of each habituation bout (x-axis) shown in b. Compact letter display above rainclouds indicates significant reduction in motor activity across habituation bouts (p<0.05, Kruskal-Wallis rank sum test). (**d, e**) More frequent stimulation results in more rapid/pronounced response decrement. Line graph shows the motor activity (y-axis) of 5-dpf zebrafish larvae over a sequence of 30 consecutive 1-second acoustic stimuli (300 Hz, 100% volume; x-axis) with different ISIs. Data is median ± 95% CI (*n* = 96). Raincloud graph shows the habituation scores (y-axis) for different ISIs (x-axis) shown in d. Habituation scores represent the cumulative motor activity per individual during stimuli 21-30 relative to the cumulative motor activity summed across stimuli 1-10 and 21-30. Compact letter display above rainclouds indicates significant

differences between ISIs ($p<0.05$, Kruskal-Wallis rank sum test). (**f, g**) Less intense stimuli result in more rapid/pronounced response decrement. Line graph shows the motor activity (y-axis) of 5-dpf zebrafish larvae over a sequence of 30 consecutive 1-second acoustic stimuli (300 Hz, ISI = 1 s; x-axis) at different nominal volume levels. Motor activity was scaled to the median response to the first acoustic stimulus per volume group to account for differences in baseline startle activity. Individuals that did not react to any of the 30 acoustic stimuli, were excluded. Data is median ± 95% CI ($n = 74$). Raincloud graph shows the cumulative motor activity during the first two stimuli scaled to the overall activity across all 30 stimuli (y-axis) for two different volume levels (x-axis) shown in f. Compact letter display above rainclouds indicates significant differences between volume levels ($p<0.05$, Kruskal-Wallis rank sum test). (**h-k**) Accumulation of habituation beyond asymptotic level. Line graphs in h and j show the motor activity of 5-dpf zebrafish larvae (y-axis) over two subsequent habituation bouts, each consisting of a sequence of 30 and 60 consecutive 1-second acoustic stimuli (300 Hz, 100% volume, ISI = 1 s; x-axis), respectively. Data is median ± 95% CI ($n = 96$). Raincloud graphs in i and k show the cumulative motor activity during the first five stimuli per habituation bout scaled to the overall motor activity during the first five stimuli per bout (y-axis) for two subsequent bouts (x-axis), each comprising of 30 and 60 acoustic stimuli shown in h and j, respectively. Compact letter display above rainclouds indicates significant differences between bouts ($p<0.05$, Kruskal-Wallis rank sum test). (**l, m**) A second, novel stimulus changes the response to the habituated stimulus (stimulus generalization/specificity). A different stimulus increases the decremented response to the original stimulus (dishabituation). Line graph shows the motor activity (y-axis) of 5-dpf zebrafish larvae over a sequence of 100 consecutive 1-second acoustic stimuli (300 Hz, 100% volume, ISI = 1 s; x-axis). Light was turned on during stimuli 51-75. Data is median ± 95% CI ($n = 96$). Raincloud graph shows the cumulative motor activity per 25-stimuli bin (indicated by dashed vertical lines in l). Compact letter display above rainclouds indicates significant differences between bins ($p<0.05$, Kruskal-Wallis rank sum test).